COMPUTER-AIDED DESIGN AND MANUFACTURING OF AN AXIAL FAN

A Master's Thesis

Presented by

Özgür ÇEÇEN

to

the Graduate School of Natural and Applied Science

of Middle East Technical University

in Partial Fulfillment of the Degree of

MASTER OF SCIENCE

in

MECHANICAL ENGINEERING
ANKARA
November 1993

Approval of the Graduate School of Natural and Applied Sciences

Prof. Dr. İsmail TOSUN

for Director

I certify that this thesis satisfies all the requirements as a thesis for the degree of Master of Science .

Prof. Dr. Rüknettin OSKAY

Chairman of the Department

We certify that we have read this thesis and that in our opinion it is fully adequate , in scope and quality , as a thesis of Master of Science in Mechanical Engineering .

Prof. Dr. M. Haluk AKSEL

Supervisor

Examining Committee in Charge :

Prof. Dr. Ahmet Ş. ÜÇER (Chairperson)

Prof. Dr. M. Haluk AKSEL (Supervisor)

Prof. Dr. Nafiz ALEMDAROĞLU (Hav. Müh.)

Doç. Dr. Kahraman ALBAYRAK

Y. Doç. Dr. Tahsin ÇETİNKAYA

ABSTRACT

COMPUTER-AIDED DESIGN AND MANUFACTURING OF AN AXIAL FAN

ÇEÇEN , Özgür
M . S . in Mechanical Engineering
Supervisor : Prof. Dr . M . Haluk AKSEL
November , 1993 , 70 pages

In this study , an axial fan is first designed by means of a computer code . The computer code is needed to decrease the time for the design operations and to give accurate results . The computer code uses QBASIC Programming Language . The computer code not only performs the design calculations but also gives the drawings of the top and the side view of the fan . It also gives the blade orientations at different divisions and the cross-sectional view of a blade at the hub side . After the design calculations are performed , the manufacturing of the axial fan is started by using the design results obtained from the output of the computer code . The manufacturing of the designed fan is carried out in three steps ; namely making the model of the fan , sand casting of the fan and turning operations . The model of the axial fan is made by wood and Aluminum . The hub of the fan is modelled by using wood , on the contrary , the models of the blades are made by Aluminum . The reason that Aluminum is used for eight blades is just for duplicating the blade profile which is wood . Owing to its physical and strength characteristics the axial fan is casted from Aluminum . As a final step , the performance of the manufactured axial fan is evaluated according to ASHRAE (American Society of Heating , Refrigerating and Air Conditioning Engineers) Standard 51-75 . The performance experiments are repeated several times in order to determine the performance curves of the manufactured axial fan accurately . There are some deviations between the designed performance variables and experimentally obtained performance variables . These deviations are due to the errors occured in the manufacturing and performance evaluation steps .

Keywords : Axial Fan , Computer-aided Design , Performance Tests

Science Code : 625.02.05

ÖZ

BİLGİSAYAR DESTEKLİ EKSENEL FAN TASARIMI VE İMALATI

ÇEÇEN , Özgür
Yüksek Lisans Tezi . Makina Mühendisligi Ana Bilim Dali
Tez Yöneticisi : Prof . Dr . M . Haluk AKSEL
Kasim , 1993 , 70 sayfa

Bu çalismada ilk önce bir bilgisayar programi kullanilarak eksenel bir fan tasarimi yapilmiştir . Tasarim hesaplarinin süresini azaltmak ve doğru sonuçlar elde etmek için bilgisayar programina gereksinim duyulmuştur . Bilgisayar programinda QBASIC programa dili kullanilmiştir . Bilgisayar programi tasarim hesaplamalarini yapmakla beraber eksenel fanin üst ve yan görünüşlerini de vermektedir . Ayrica program değişik çaplardaki kanat yerleşimlerini ve kanatlarin göbek üzerindeki kesit görünüşlerini de sağlamaktadir . Tasarim hesaplamalari bitirildikten sonra bilgisayar çiktisindan yararlanilarak fanin imalati başlatilmiştir . Tasarlanan eksenel fanin imalati üç aşamada gerçekleştirilmiştir , sirasiyla , fan modelinin yapilmasi , döküm ve tornalama işlemleridir . Eksenel fanin modeli ahşap ve Aluminyum'dan yapilmiştir . Fanin modelinin göbeği ahşaptan , kanatlarin modelleri ise Aluminyum'dan imal edilmiştir . Aluminyum'un kullanilma nedeni ahşaptan modeli yapilan sekiz kanadin kopye edilmesi amacidir . Eksenel fan fiziksel ve mukavemet özelliklerinden dolayi Aluminyum 'dan dökülmüştür . Yüzey bozukluklarini ve ölçülerdeki sapmalari ortadan kaldirmak amaciyla tornalama operasyonlari gerçekleştirilmistir . Sonuç olarak , imal edilen eksenel fanin performansi ASHRAE (American Society of Heating , Refrigerating and Air Conditioning Engineers) 'nin 51-75 nolu standardina göre değerlendirilmiştir . İmal edilen eksenel fanin performans eğrilerinin doğru olarak belirlenmesi için performans testleri bir çok defa tekrar edilmiştir . İmal edilen fanın deneysel olarak elde edilen performans değişkenleri ve tasarlanan performans değişkenleri arasinda sapmalar olduğu görülmüştür . Bu sapmalarin nedeni imalat ve performans değerlendirme işlemlerinde yapilan hatalardir .

Anahtar Kelimeler : Eksenel Fan , Bilgisayar Destekli Tasarim
Performans Testleri

Bilim Sayisal Kodu : 625.02.05

ACKNOWLEDGEMENTS

I am grateful to Prof . Dr . M . Haluk AKSEL , Dr . Kahraman ALBAYRAK and Prof . Dr . O . Cahit ERALP for providing me with their generous and unstinted assistance during the studies of this thesis .

My grateful acknowledgements are due also to Mr . Taner KORKMAZ and Mr . Cemalettin ŞAHİNGÖZ for their help in laboratory work.

TABLE OF CONTENTS

LIST OF TABLES

LIST OF FIGURES

LIST OF SYMBOLS

Q	Volumetric Flow Rate	m^3/s
Δp_t	Total Pressure Difference	N/m^2
N	Rotational Speed	rps
H	Head	mmWG
g	Gravitational Acceleration	m/s^2
d_1	Inside Diameter of the Fan	m
d_2	Outside Diameter of the Fan	m
IP	Power to drive the Fan	W
IP_0	Power output of the Fan	W
V	Velocity of the Fluid	m/s
A	Cross-sectional Area	m^2
U	Peripheral Velocity	m/s
Z	Number of the Blades	
t	Pitch	m
A_a	Aerofoil Area	m^2
p	Velocity Pressure	N/m^2
C_L	Lift Coefficient	
C_D	Drag Coefficient	
W	Relative Velocity	m/s
L	Lift Force	N
D	Drag Force	N
ℓ	Chord Length of the Blade	m
v	Local Excess	deg
R	Radius of Curvature	m
s	Blade Thickness	m
F	Force	N
$\dot{m}$	Mass Flow Rate	kg/s
r	Radius	m
F_c	Centrifugal Force	N
n	Factor of Safety	
D	Diameter of the duct	m
σ	Speed Coefficient	
δ	Diameter Coefficient	
η_{tot}	Total Efficiency	
γ	Hub Ratio	
ε	Glide Angle	deg
ρ	Density	kg/m^3

α , β	Blade Angles	deg
μ	Excessive Bending	
ν_∞	Overall Deflection of the Flow	deg
$\Delta\beta$	Ultimate Opening Angle	deg
Ω	Tensile Stress	N/m^2

Subcripts

1	Inlet , inside
2	Outlet , outside
m	Meridional , mean
∞	Mean velocity direction
θ	Tangential direction

CHAPTER I

INTRODUCTION

1.1 Introduction

The purpose of a turbomachine is either changing the energy available in fluid to mechanical energy , as in the case of turbines or increasing the energy of the fluid from a lower level to a higher one such as in pumps or fans . A turbomachine has primarily an impeller on which several number of blades are mounted . The working fluid flows between the blades continously . Therefore , the ability of the turbomachine depends on the pressure distribution on the blades . The occurence of the forces on the blades of the impeller is considered as a result of the change of direction of the flow by the blades . This change is due to the presence of inertial forces in the working fluid . These blade forces are basically similar with the ones appeared on an isolated aerofoil as lift forces from the point of view of their reason of occurence . The large impellers used in wind mills are good examples expressing the above situation . In these mills , the wind direction in other words the direction of air flow is changed by means of the impeller . Moreover , the same phenomenon can be realised in the aeroplane and ship propellers are driven by an external power input . The pressure distribution on the blades which brings about a thrust force causes the ship or the aeroplane to move forward .

Turbomachines basically have rotative elements in comparison to reciprocating machines operating with the theory of positive displacement such as internal combustion engines . In reciprocating machines , the state of working fluid changes as it goes through the machine owing to the change in the internal volume of the machine . On the contrary , the working fluid passes through the machine in a steady manner in turbomachines . To be more precise , the change of the pressure of the fluid is due to the dynamic causes in these machines . When a comparison between the fields of application of reciprocating machines and turbomachines is done , it is observed that both of them may be used mainly in the same application areas . As an example the compression of gases can be achieved by means of either a rotating or a reciprocating machine . Furthermore , both a centrifugal or a reciprocating pump are easily utilized for transferring water from a lower elevation to a higher one . Also gas turbines which are considered as an alternative to internal combustion engines can be used primarily in the same area where the reciprocating steam engines are in use .

It was proved that turbomachines are more effective and efficient than the reciprocating ones when high volumetric flow rates are required . However , the applications with low flow rates are usually performed with reciprocating

machines . In turbomachines high energy transfers could be achieved with smaller installment area requirement compared with the large and heavy reciprocating engines . Since the developments are towards designing power stations with large power output , low installation costs and high efficiencies , the importance of the turbomachines is increased in industrial applications .

A wide variety machines known to trade under several names such as fans , blowers and compressors create the gas pumping turbomachinery . In all of them the gaseous fluid is compressed and moved by the dynamic action of the rotating blades of one or several impellers . These impellers impart the velocity and the pressure to the working fluid . When the low pressure rise and high flow rate requirements are considered , fans are basically used . The increase of gas density in fans often exceeds 7 percent . When medium pressure increases are required , a name applied to the machine is a blower . A blower can be known as "exhauster" if it is used to remove gas form a process or a container and to discharge it to the atmosphere . On the other hand , the blower may be referred as a "booster" if it is used to increase the pressure in the system that is already above the atmospheric pressure . For instance , the blowers mounted on the natural gas pipelines can be referred as boosters . For higher discharge pressures the term used is a "compressor" . The physical dimensions and the methods of manufacturing are different for each of these gas pumping turbomachines .

Fans may be considered as one of the known gas pumping turbomachines . A fan is a machine for increasing its energy content of a gaseous fluid . This energy enables the movement or flow of the gas against various degrees of resistance . The function of a fan is to move air or gases through distribution systems and apparatus required for conditioning of the gas medium , such as systems for heating , ventilating and air conditioning of buildings . In systems for drying and cooling of materials and products , for pneumatic conveying of materials , for industrial process work , for mine and tunnel ventilation and for forced and induced draft of steam generation plants , various types of fans are used. The fan consists of a rotating member called the impeller and a stationary member called the housing or the duct . The housing is provided with an intake opening (inlet) and with a discharge opening (outlet) . The working fluid enters at the inlet , flows continously between the blades and discharges at the outlet . Fans are normally classified as centrifugal or axial . Centrifugal fans are used in application which require greater pressure rise compared to axial fans . Axial fans are usually applied to move large quantities of air at low pressure .

Centrifugal fans are classified according to their blade configurations : as radial , forward-curved and backward-curved as shown in Figure 1.1 .

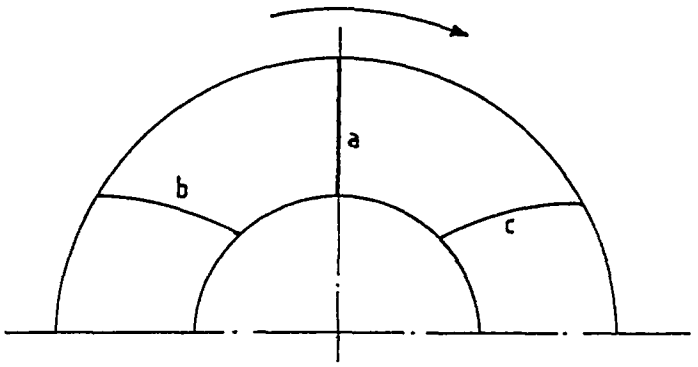

Figure 1.1 Centrifugal fan types : a)Radial b)Backward-curved c)Forward-curved

There are two types of axial flow fans , namely tube-axial and vane-axial . Tube-axial fans are designed for a wide range of volumetric flow rates at medium pressure increases . These fans primarily consist of an impeller enclosed in a cylindrical duct which collects and directs the air flow . A helical or screw-like motion of air can be seen at the discharge of the fan . Figure 1.2 illustrates schematically a tube-axial fan the typical flow pattern of air .

Vane-axial fans are characterized by air guide vanes on the discharge side . These are also known as stators or diffuser vanes . These stators provide the reduction in turbulence and thus improve the performance characteristics of the fan ; e.g. efficiency . The air flow without swirl is the flow pattern in these type of axial flow fans , as shown schematically in Figure 1.3 . Vane-axial fans can produce higher pressure rise compared to tube-axial fans . Also inlet guide vanes can be used in the vane-axial fans to improve the performance charactaristics further .

The main part of the tube-axial and vane-axial fans is the impeller which consists of a hub and several number of blades as shown in Figure 1.2 .

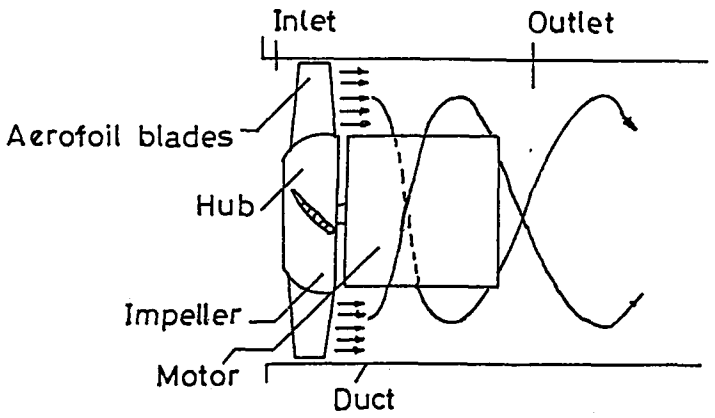

Figure 1.2 Tube-axial fan

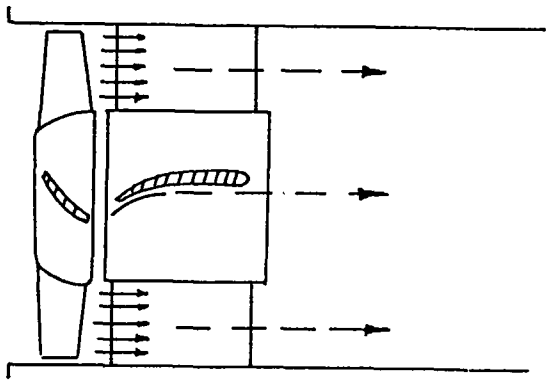

Figure 1.3 Vane-axial fan

The impeller is usually connected to an electric motor directly . But , in some applications the connection is achieved by means of V-belts .

In industry , both tube-axial and vane-axial fans are used for supplying air for oil and gas burners or combustion furnaces . They are also used in ventilating process plants . In the cooling towers , the tube-axial fans are preffered . Both of them are utilized in process drying applications .

1.2 Historical Background

In early years of this century , the fans were designed by using the practical experiences and self capabilities of the engineers . Mostly , trial and error procedures were followed to obtain best results . The design engineers used only very little fluid mechanics around 1900 . As soon as the fluid mechanics had been started to develop , the theory about the fans began to advance in 1930's . They combined the advancing theory about the fans with the accumulated practical experiences to obtain efficient design procedures . In 1940's , a German professor , Carl Pfleiderer [1] did considerable work on turbomachinery at Braunschweig Technical University in Germany . He determined methods for designing turbines , pumps , compressors and fans . Between 1952 and 1960 , he published several papers about the design of fans . After his deadth in 1960 , another German professor at the same university , Hartwig Petermann [2] improved the Pfleiderer's methods . He applied the experimental results of the researches performed at the Pfleiderer Institute of Flow Machines to the developed methods . In 1950's , there were also considerable research on turbomachinery . Bruno Eck [3] , a German scientist and engineer obtained efficient procedures for designing fans . Mainly , his purpose was to eliminate the trial and error procedures and to apply his theoretical and experimental investigations to the design of fans . In 1959 , John N.Alden [4] , an American scientist , developed design procedures for fans used in industrial exhaust systems . He combined fan design principles with duct design principles . In 1983 , an Australian scientist and engineer , R.Allan Wallis [5] found design procedures for axial flow fans used in air handling systems . Also , he explained the axial fan

design methods in combination with the air handling duct design procedures . The advancing computer technology is also used for decreasing the design period and increasing the accuracy . Furthermore , the computer-aided design (CAD) procedures become popular for the past ten years .

1.3 Present Work

The purpose of this thesis is to design an axial fan with the aid of a computer program , to manufacture it and finally test its performance by using a standard testing method .

In this study , a tube-axial fan with a given volumetric flow rate and pressure difference is designed by means of a computer code . Modelling and sand casting processes are applied for manufacturing the fan . The performance of the fan is evaluated by using one of the standard test procedures , namely ASHRAE (American Society of Heating Refrigerating and Air Conditioning Engineers) Standard 51-75 . Moreover , the comparison between the designed and manufactured fan is also performed .

In Chapter II , the design procedure is explained step by step with the given input parameters. Chapter III explains the methods for manufacturing of the designed fan . In Chapter IV, the test apparatus used to evaluate the performance of the fan and the methods for flow and pressure measurements are considered . Chapter V involves the results obtained from the performance tests . Finally , Chapter VI provides the discussions about the results , comparisons between the designed and manufactured fans and conclusions reached after the experiments .

CHAPTER II

DESIGN PROCEDURE

In this chapter , the design procedure for axial fans is explained . The theory behind the design procedure is provided before explaining the design steps .

2.1 Theory

As it is stated in Chapter I , the axial fan consists of a rotating member called the impeller and a stationary member called the duct . The duct is provided with an intake opening (inlet) and with a discharge opening (outlet) . The impeller consists of a hub and several number of blades . These blades are mounted on the hub of the impeller . The working fluid , which is generally air , enters at the inlet , flows continously between the blades and discharges at the outlet . There are two types of axial fans , namely tube-axial and vane-axial . Tube-axial fans are designed for a wide range of volumetric flow rates at medium pressure increases . These fans primarily consist of an impeller enclosed in a cylindrical duct which collects and directs the air flow . Vane-axial fans are characterized by air guide vanes on the discharge side . These guide vanes provide the reduction in turbulence and thus improve the performance characteristics of the fan . Vane-axial fans can produce higher pressure rise and volumetric flow rate compared to tube-axial fans .

Consider an impeller of the axial fan rotating in a cylindrical duct as shown in Figure 2.1 . The blades are in the shape of aerofoils .The cross-sectional view of a blade varies from the hub side to the tip side . If the cross-sectional views of all blades at a fixed diameter are developed on a plane , cascades of the aerofoils are obtained . This is shown in Figure 2.2.

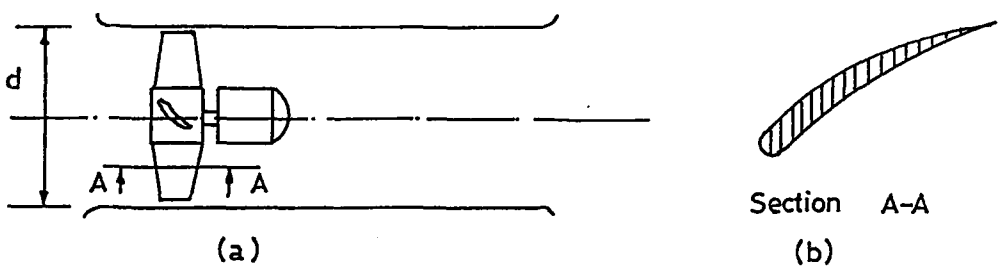

Figure 2.1 Cross-sectional view of one blade on the impeller

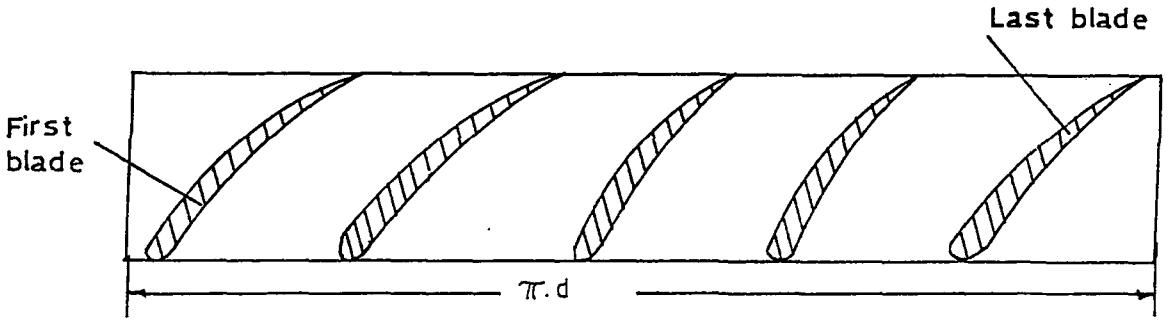

Figure 2.2 Cascade of the aerofoils

The theory about the flow between the cascades of the aerofoils is explained in the following paragraphs :

Let the air at an angle of α_1 enter to a stationary cascade as shown in Figure 2.3 . The direction of the air flow is deflected from α_1 to α_2 at the disharge of the cascade . The air velocity at the inlet of the cascade is V_1 and V_2 at the outlet of the cascade .

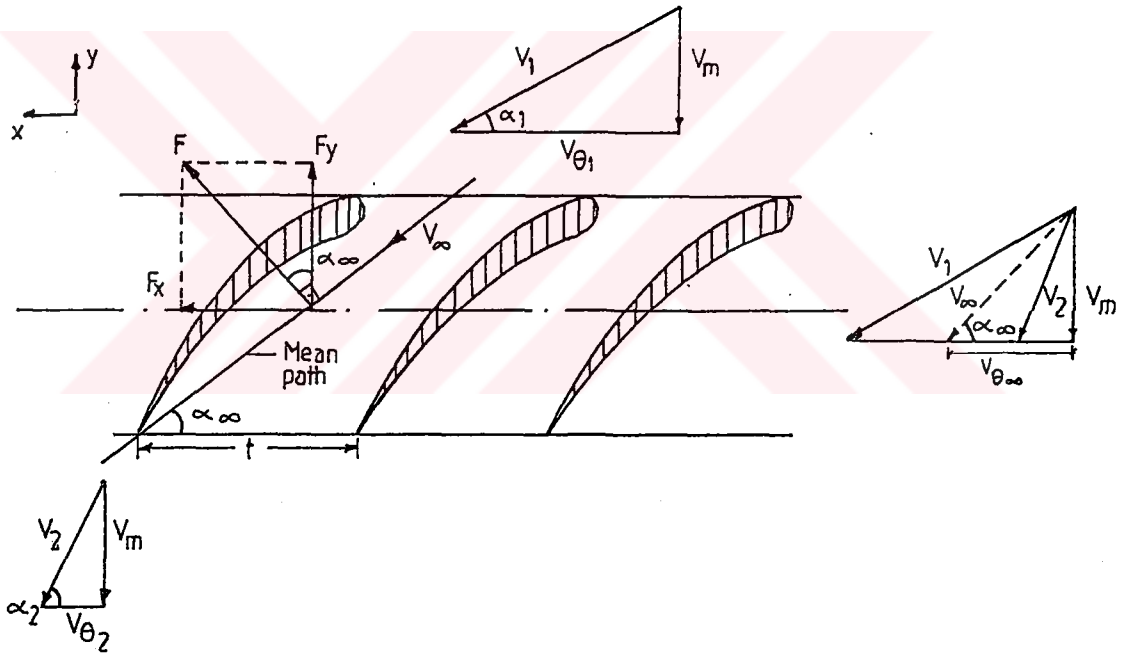

Figure 2.3 Velocity diagrams and forces in a stationary cascade

The velocity diagrams at the inlet and outlet of the cascade are also shown in Figure 2.3 . The velocity component V_m is called as the meridional velocity and is perpendicular to the cascade plane . If the continuity equation is applied between the inlet and outlet of the cascade , the following results will be obtained for incompressible flow :

$$V_{m1} \cdot t \cdot b = V_{m2} \cdot t \cdot b \tag{2.1}$$

so that ,

$$V_{m1} = V_{m2} = V_m \tag{2.2}$$

where t is the distance between the blades which is called as the pitch and b is the width perpendicular to the plane of the drawing .

From Figure 2.3 ,

$$V_m = V_1 \cdot \sin \alpha_1 = V_2 \cdot \sin \alpha_2 \tag{2.3}$$

Using Bernoulli Equation between the inlet and outlet of the cascade and , neglecting the frictional effects ,

$$p_2 - p_1 = \Delta p = \frac{\rho}{2} \cdot \left[\left[V_1 \right]^2 - \left[V_2 \right]^2 \right] \tag{2.4}$$

where Δp is the static pressure difference between the inlet and outlet of the cascade and ρ is the density of the air . This pressure difference creates in the axial direction as shown in Figure 2.3 . Using linear momentum equation in y direction ,

$$F_y = \frac{\rho}{2} \cdot \left[\left[V_{\theta 1} \right]^2 - \left[V_{\theta 2} \right]^2 \right] \cdot t \cdot b \tag{2.5}$$

where $V_{\theta 1}$ and $V_{\theta 2}$ are the velocities in the tangential or peripheral direction at the inlet and outlet of the cascade.

The force in the direction of the axial axis can be calculated by using the momentum equation ; since the mass flow rate through the division , t is

$$\dot{m} = \rho \cdot t \cdot b \cdot V_m \tag{2.6}$$

so that ,

$$F_x = t \cdot b \cdot V_m \cdot \rho \cdot \left[V_{\theta 2} - V_{\theta 1} \right] \tag{2.7}$$

F_x is the force on the air by the cascade whereas the opposing force $F_{x'}$ is exerted by the air on the cascade . Thus ,

$$F_{x'} = t \cdot b \cdot V_m \cdot \rho \cdot \left[V_{\theta 1} - V_{\theta 2} \right]$$

One can easily find the magnitude of the resultant of the two forces , that is ,

$$F=\sqrt{\left[F_x\right]^2+\left[F_y\right]^2}$$

Substituting ,

$$\left[V_\theta\right]_\infty=\frac{V_{\theta 1}+V_{\theta 2}}{2}$$

$$\left[V_\infty\right]^2=\left[\left[V_\theta\right]_\infty\right]^2+\left[V_m\right]^2$$

One can get ,

$$F=\rho\cdot t\cdot b\cdot\left[V_{\theta 1}-V_{\theta 2}\right]\cdot V_\infty \tag{2.8}$$

and the direction ,

$$\cot\alpha_\infty=\frac{\cot\alpha_1+\cot\alpha_2}{2} \tag{2.9a}$$

where ,

$$\vec{V}_\infty=\frac{\left[\vec{V}_1+\vec{V}_2\right]}{2} \tag{2.9b}$$

The direction of this average velocity is called as the mean path . The direction of the resultant force F is perpendicular to the mean path as shown in Figure 2.3 .

Now , consider a rotating impeller onwhich several number of the blades are mounted . The velocity U is the peripheral velocity as illustrated in Figure 2.4 . The cascade of aerofoils are also obtained if the cross-sectional views of all blades at a specific diameter are developed on a plane . The cascade of aerofoils moves along the cascade axis . The velocity of the cascade is equal to U . This is shown in Figure 2.5 .

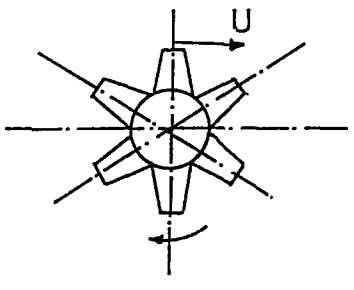

Figure 2.4 A rotating impeller having the peripheral velocity , U

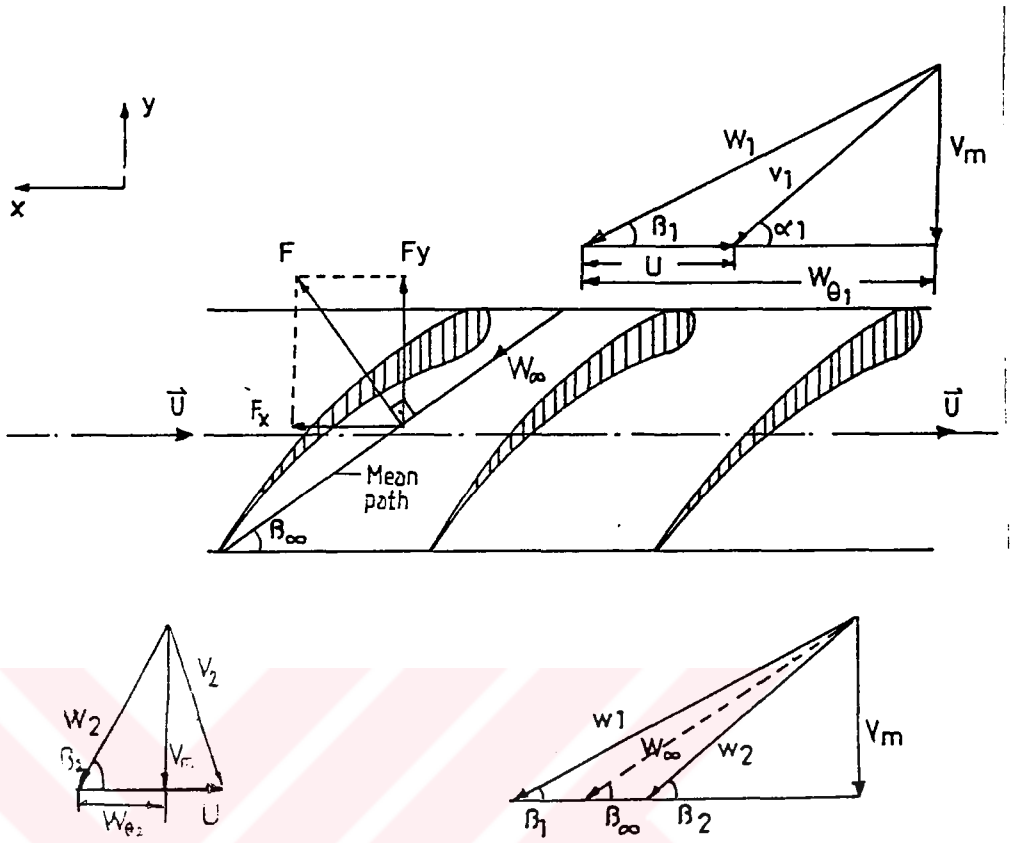

Figure 2.5 Velocity diagrams and forces in a moving cascade

From velocity triangles at the inlet and at the outlet of the cascade ,

$$\vec{V}_1=\vec{W}_1+\vec{U} \tag{2.10}$$

$$\vec{V}_2=\vec{W}_2+\vec{U} \tag{2.11}$$

where $\vec{W}_1$ and $\vec{W}_2$ are the relative velocities at the inlet and outlet of the cascade.

If one moves along with the cascade , he only sees a stationary cascade with the intake an discharge velocities of W_1 and W_2 similar to the stationary cascade . The resultant force acting on the blade is perpendicular to the direction of W_∞ (mean velocity) . W_∞ is the vector average of the relative velocities W_1 and W_2 ; that is ,

$$\vec{W}_\infty=\frac{\left[\vec{W}_1+\vec{W}_2\right]}{2} \tag{2.12}$$

Similar to the stationary cascade , using continuity , extended Bernoulli , momentum equations and velocity diagrams shown in Figure 2.5 , one can get the following results :

$$p_2 - p_1 = \Delta p = \frac{\rho}{2} \cdot \left[\left[W_1 \right]^2 - \left[W_2 \right]^2 \right] \tag{2.13}$$

$$F_y = \frac{\rho}{2} \cdot \left[\left[W_1 \right]^2 - \left[W_2 \right]^2 \right] \cdot t \cdot b \tag{2.14}$$

$$F_x = t \cdot b \cdot V_m \cdot \rho \cdot \left[V_{\theta 1} - V_{\theta 2} \right] \tag{2.15}$$

$$F = \rho \cdot t \cdot b \cdot W_\infty \cdot \left[W_{\theta 1} - W_{\theta 2} \right] \tag{2.16}$$

The work done by the cascade on the air is equal to the force F_x times the peripheral velocity U . One can imagine that this work is also equal to the work which is done for raising the same weight of air to a height , H . Therefore ,

$$F_x \cdot U = \dot{m} \cdot H \tag{2.17}$$

Solving for H ,

$$H = \frac{U}{g} \cdot \left[V_{\theta 2} - V_{\theta 1} \right] \tag{2.18}$$

where H is the head . In fans , it is more practical to work with a pressure increase Δp_t instead of the head .Thus ,

$$H = \frac{1}{\rho \cdot g} \cdot \Delta p_t \tag{2.19}$$

Equating both Equations (2.18) and (2.19) and solving for Δp_t,

$$\Delta p_t = \rho \cdot U \cdot \left[V_{\theta 2} - V_{\theta 1} \right] \tag{2.20}$$

The above equation is called as " Euler Turbine Equation" [6] .

The velocity triangles at the inlet and at the outlet of the axial fan with no air guide vanes are shown in Figure 2.6 . There are air guide vanes at the inlet and at the outlet of the axial fans in some applications . The shapes of the velocity triangles at the inlet and at the outlet of the axial fan are illustrated in Figure 2.7 .

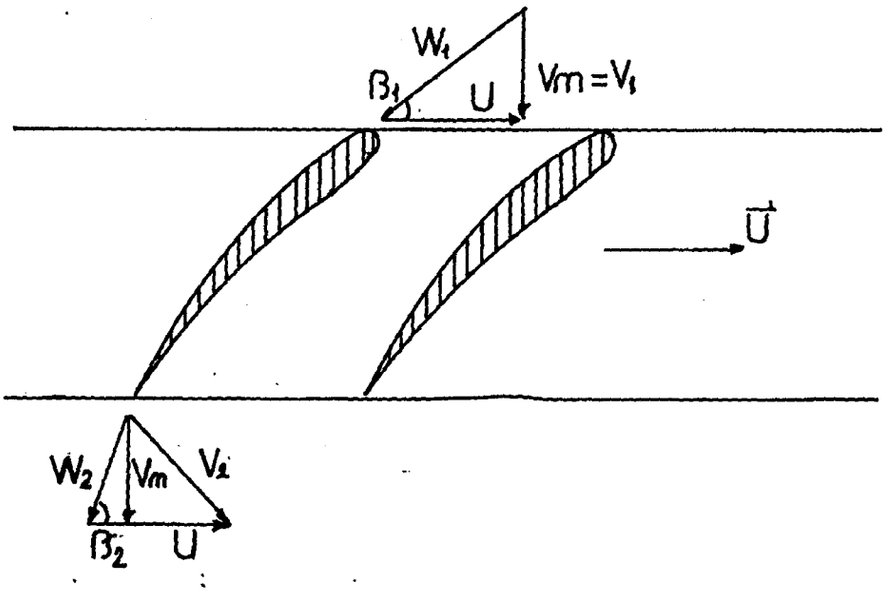

Figure 2.6 The impeller with no guide vanes

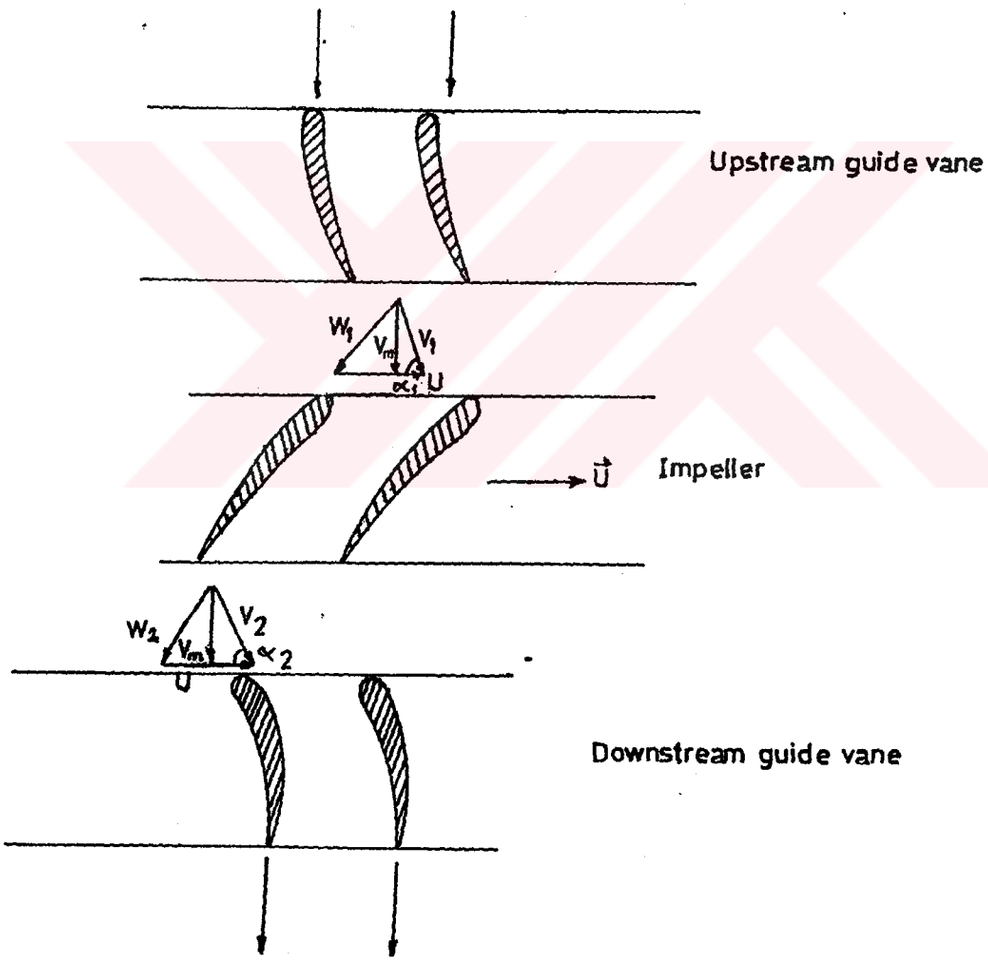

Figure 2.7 The upstream guide vane , impeller and downstream guide vane arrangement

From the beginning of Chapter II up to this point , the total pressure increase is calculated by using the peripheral velocity , the tangential velocities at the inlet and/or outlet of the cascade . The shape of the aerofoils is not taken into account . At this point , consider an aerofoil which is placed in an air stream having velocity , w as shown in Figure 2.8 . It can be considered that the aerofoil moves in the still air with a velocity , w .

The air flow exerts a force on the aerofoil having two components . One of them is perpendicular to the flow path and it is called as the lift force , L . The other one is called as the drag force , D and its direction is parallel to the air flow . The drag force is smaller than the lift force . Therefore ,

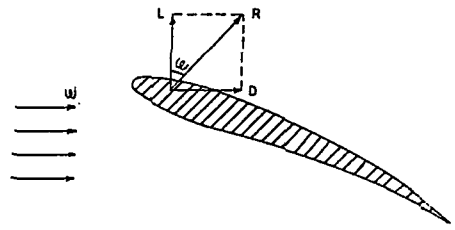

Figure 2.8 An aerofoil placed in a free air stream of velocity , w

$$L = C_L \cdot p \cdot A_a \tag{2.21}$$

$$D = C_D \cdot p \cdot A_a \tag{2.22}$$

where A_a is the aerofoil area in meter square , p is the velocity pressure in Newtons per meter square , ε is the glide angle , C_L is the lift coefficient and C_D is the drag coefficient . In order to calculate the total pressure across the cascade of the aerofoils , one can refer the cascade arrangement as shown in Figure 2.9 .

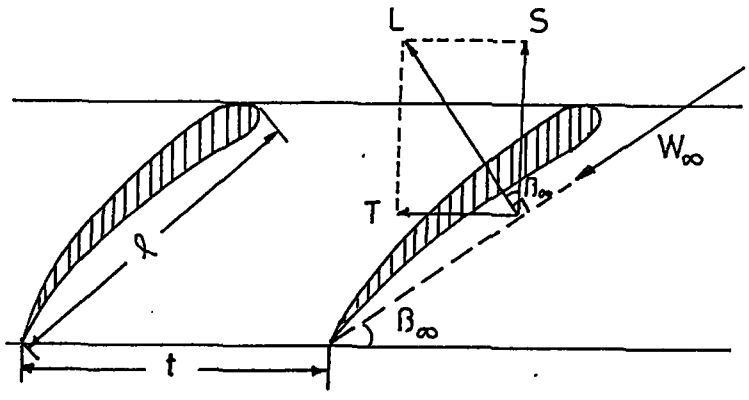

Figure 2.9 Forces acting on a cascade of aerofoils without considering the friction [7]

The aerofoil friction is neglected and thus , the drag force is zero . The velocity or dynamic pressure is ,

$$p=\frac{\rho}{2}\cdot\left[W_{\infty}\right]^{2} \tag{2.23}$$

and the aerofoil area is,

$$A_a=l\cdot b \tag{2.24}$$

where ℓ is the chord length of the aerofoil or the blade and b is the width perpendicular to the plane of drawing . From Figure 2.9 ,

$$T=L\cdot\sin\beta_{\infty} \tag{2.25}$$

$$S=L\cdot\cos\beta_{\infty} \tag{2.26}$$

Also using the momentum principle between the outlet and inlet of the cascade ,

$$T=\dot{m}\cdot\Delta V_{\theta} \tag{2.27}$$

where the mass flow rate is ,

$$\dot{m}=t\cdot b\cdot V_m\cdot\rho \tag{2.28}$$

where V_m is the meridional velocity .

Substituting Equation (2.28) into Equation (2.27) ,

$$T=t\cdot b\cdot V_m\cdot\rho\cdot\Delta V_{\theta} \tag{2.29}$$

From Figure 2.5 ,

$$V_m=W_{\infty}\cdot\sin\beta_{\infty} \tag{2.30}$$

Substituting Equation (2.30) into Equation (2.29) ,

$$T=t\cdot b\cdot W_{\infty}\cdot\sin\beta_{\infty}\cdot\rho\cdot\Delta V_{\theta} \tag{2.31}$$

Combining Equations (2.21) , (2.23) , (2.24) and (2.25) ,

$$T=\frac{\rho}{2}\cdot C_L\cdot l\cdot b\cdot \sin\beta_\infty\cdot\left[W_\infty\right]^2 \tag{2.32}$$

Equating Equations (2.31) and (2.32) , one may obtain ,

$$t\cdot\Delta V_\theta=\frac{C_L}{2}\cdot l\cdot W_\infty \tag{2.33}$$

Substituting Euler Turbine Equation, given by Equation (2.20) into Equation (2.33) ,

$$\frac{t}{\rho\cdot U}\cdot\Delta p_t=\frac{C_L}{2}\cdot l\cdot W_\infty \tag{2.34}$$

Substituting Equation (2.30) into Equation (2.34) and rearranging ,

$$\Delta p_t=\rho\cdot l\cdot U\cdot V_m\cdot\frac{C_L}{2\cdot t\cdot\sin\beta_\infty} \tag{2.35}$$

If the aerofoil friction is considered , the drag force will then exist . The forces acting on the aerofoil are shown in Figure 2.10 .

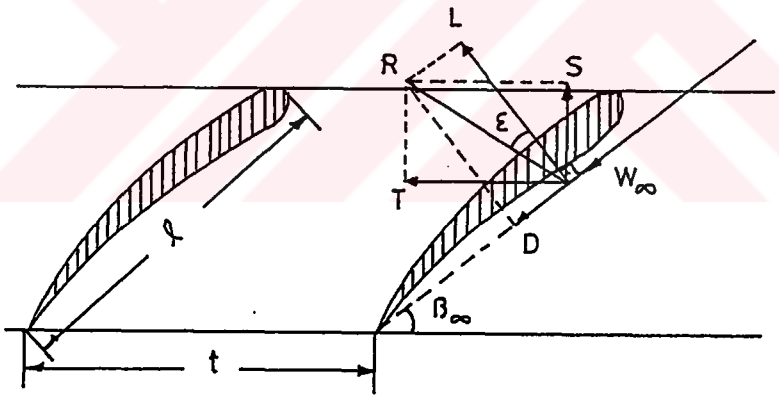

Figure 2.10 Forces acting on an aerofoil cascade considering the friction

If η_{tot} is the total efficiency of the axial fan , the aerofoil blades of the fan must exert a higher Δp_t, namely $\Delta p_t/\eta_{tot}$. Therefore , Equation (2.35) becomes ,

$$\Delta p_t=\rho\cdot l\cdot U\cdot V_m\cdot\eta_{tot}\cdot\frac{C_L}{2\cdot t\cdot\sin\beta_\infty} \tag{2.36}$$

It is understood that the total pressure increase can also be calculated by using Equation (2.36) . However , the chord length of the blade and lift coefficient must be known beforehand .

Now the design procedure for the axial fan will be explained step by step :

2.2 Design Procedure

As it is stated before , the blades of the axial fans are in the shape of aerofoils . The purpose of the design is profiling these aerofoils so that the required volumetric flow rate and the total pressure increase are obtained . In this study , the blades are not considered in the shape of aerofoils . The thickness of the blade is considered as constant throughout the cross-section at all radii .

2.2.1 Design Inputs

In general , the volumetric flow rate , Q and the total pressure increase, Δp are given . The choice of the driving machine determines the rotational speed , N , of the impeller . Thus , Q , Δp and N are given as design inputs .

2.2.2 Calculation of Dimensionless Parameters Related to the Design

i) Calculation of the Speed Coefficient and Diameter Coefficient

In practice , a given volumetric flow rate , Q and a pressure increase Δp can be produced by various fans which are widely different in their dimensions and also in the shape of their flow passage . The cost of a fan is usually dependent upon its size , and the importance of this fact for the clients can not be omitted . One specific speed gives the best efficiency for a certain shape of a machine . Depending on the specific speed , the meridional shape of the impeller changes . For low specific speeds , the most efficient fan is the one with a radial impeller , namely a centrifugal fan . For medium specific speeds mixed flow type impellers are efficient . The most efficient impeller is an axial impeller for high specific speeds . Considering the same rotational speed , centrifugal fans are recommended for high heads but low volumetric flow rates . On the contrary , axial fans are more efficient at low heads but high volumetric flow rates .

In this study , the dimensionless parameter speed coefficient , σ is used instead of the specific speed . It should be noted that the speed coefficient is directly proportional to the specific speed . Therefore , depending on the value of σ , the meridional shape of the impeller of a fan changes . For high values of σ , the shape is axial , while , it is radial for the low σ values . This is illustrated in Figure 2.11 .

The speed coefficient , σ equals to ,

$$\sigma = N \cdot \frac{\sqrt{Q}}{(2 \cdot g \cdot H)^{0.75}} \cdot 2 \cdot \sqrt{\pi} \tag{2.37}$$

where ,

$$H = \frac{1}{\rho \cdot g} \cdot \Delta p_t$$

where N is the rotational speed in revolutions per second , Q is the delivery volume in cubic meter per second , H is the total head in meters , Δp_t is the pressure difference in Newtons per meter square , ρ is the density of fluid in kilograms per cubicmeter and g is the gravitational acceleration in meters per second square . And the diameter coefficient , δ equals to ,

$$\delta = \frac{1}{2} \cdot \sqrt{\pi} \cdot d_2 \cdot \frac{(2 \cdot g \cdot H)^{0.25}}{\sqrt{Q}} \tag{2.38}$$

where d_2 is the outside diameter in meters , Q is the delivery volume in cubic meter per second , H is the total head in meters , g is the gravitational acceleration in meters per second square .

Since the outside diameter , d_2 is not known at this step , Equation (2.38) can not be used for determining the diameter coefficient , δ .

One can use the following experimentally found diagram to obtain the diameter coefficient [9] . In Figure (2.12) , the results of the investigations of Buhning [10] and Marcinowski [11] are shown for all ranges of σ and δ .

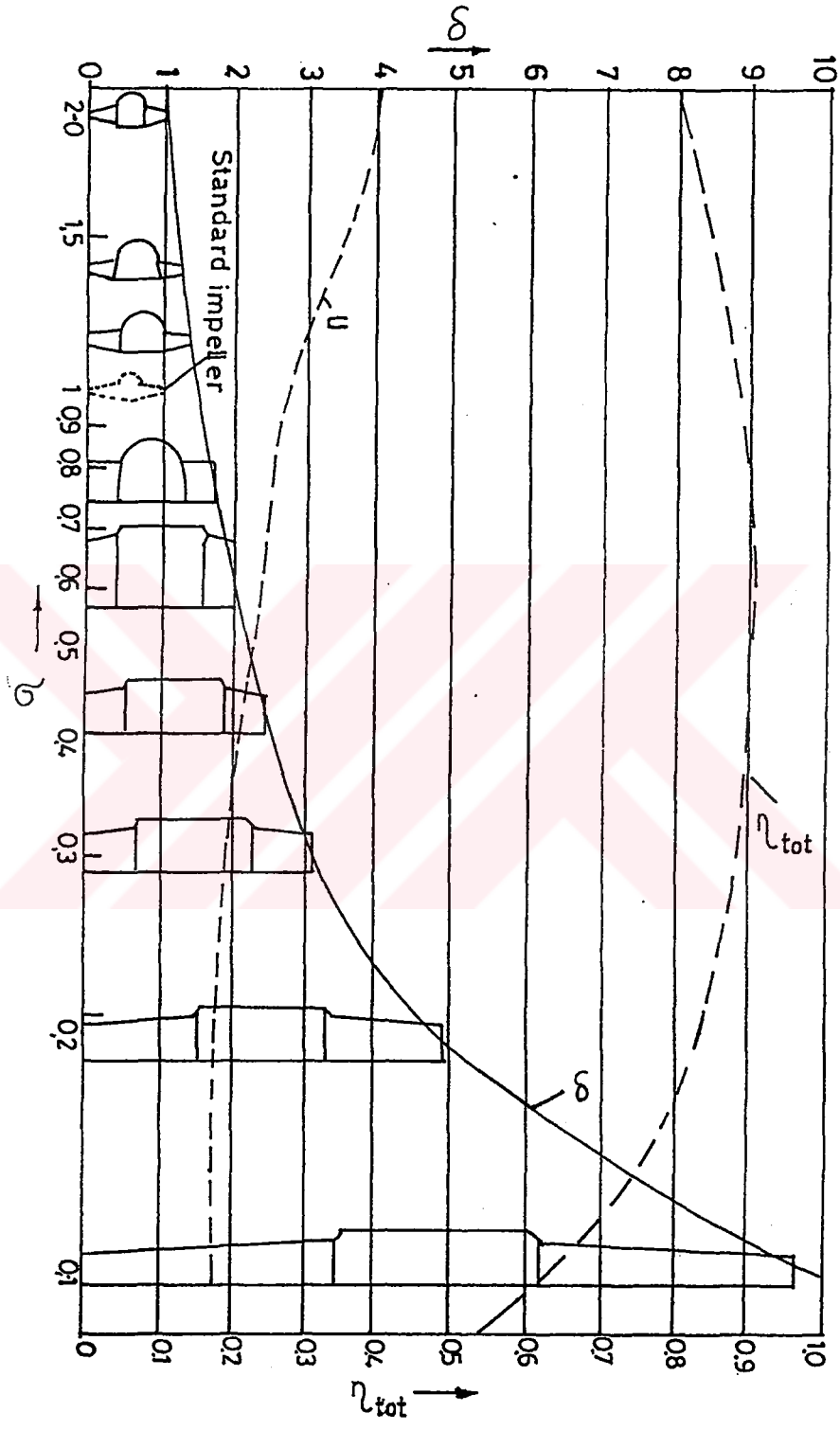

Figure 2.11 Various impellers shown on a $\sigma - \delta$ diagram [8]

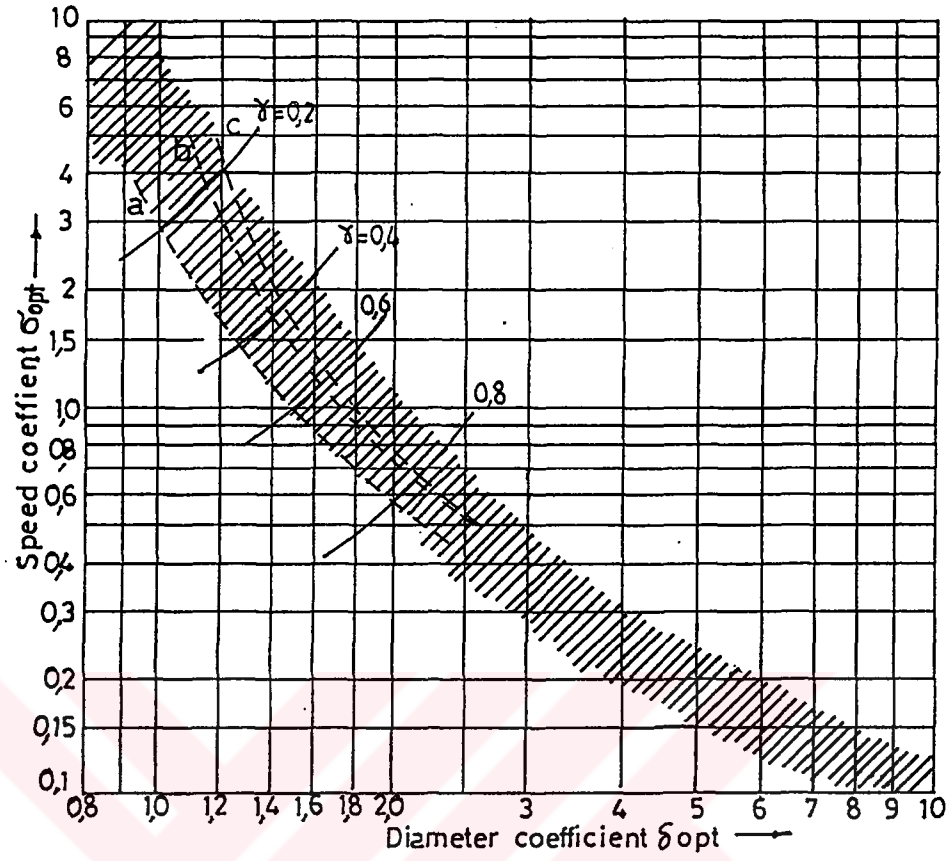

Figure 2.12 Optimum curves of the speed and volume coefficient [9]

One uses Figure 2.12 in the following way : After the speed coefficient is calculated by using Equation (2.37) , the diameter coefficient will be found with using the speed coefficient and the related arrangement type that is one of the curves labelled by a , b , c . Curve , a denotes that there is a duct after the discharge of the fan . If there are air guide vanes (stator or diffuser vane) at the discharge of the fan then curve b should be selected . Curve , c is used when the flow discharges directly after the fan . In this study , since a tube-axial is designed , there is no stator at the discharge of the fan .

ii) Calculation of the Hub Ratio

The hub ratio , γ , is defined as the ratio of the inside diameter to the outside diameter of the fan . Thus ,

$$\gamma=\frac{d_1}{d_2} \qquad (2.39)$$

The value of the hub ratio is found from Figure 2.12 [9] . The intersection point of σ line and related curve gives the value of the hub ratio .

2.2.3) Calculation of the Outside Diameter

One can calculate the outside diameter , d_2 from Equation (2.38) and subtituting Equation (2.19) as ,

$$d_2=(0.949)\cdot\delta\cdot\sqrt{Q}\cdot\rho^{0.25}\cdot\Delta p_t^{-0.25} \qquad (2.40)$$

where Q is in cubic meters per second , Δp_t is in Newtons per meter square , ρ is in kilograms per cubic meter and d_2 is in meters .

2.2.4) Calculation of the Inside Diameter

Equation (2.39) may be solved for the inside diameter d_1 as ,

$$d_1=\gamma\cdot d_2 \qquad (2.41)$$

2.2.5) Calculation of the Total Efficiency

A number of the efficiencies are used for describing the performance of the turbomachines . These are namely hydraulic , volumetric , internal and mechanical efficiencies . The hydraulic efficiency is the ratio of the actual head to the theoretical head of a fan . The difference between the theoretical and actual head is due to the losses caused by the viscosity of the flowing fluid . The volumetric efficiency is the ratio of the actual volumetric flow rate to the theoretical volumetric flow rate . The actual one is less than the theoretical one , because there is an internal leakage which occurs through the unavoidable clearance gaps between the impeller and the duct . The ratio of the output power of a fan to the internal power is called as the internal efficiency . The internal power of a fan can be obtained by subtracting the mechanical power loss from the electric motor shaft power .This mechanical power loss mainly occurs at the bearings . The mechanical efficiency is the ratio of the internal power to the shaft power or electric motor power of the fans . Finally , the total efficiency is the ratio of the output power to the power of the electric motor . Therefore ,

$$\eta_{tot}=\frac{Q}{IP}\cdot\Delta p_t \qquad (2.42)$$

where IP is the power required to drive the fan in Watts and Δp_t is the total pressure rise across the fan in Newtons per meter square .

Equation (2.42) can be more accurately determined by conducting experiments . Since IP is not known at this step , the total efficiency can be guessed directly from the experimentally determined curves , as shown in Figure 2.11 .

Using the calculated speed coefficient value , the total efficiency can be found from Figure 2.11 .

2.2.6) Calculation of the Meridional Velocity

Since uniform velocity distribution assumption is assumed at the inlet of the fan , the meridional velocity , V_m , is a calculated from the continuity equation . As a result ,

$$Q=\frac{\pi}{4}\cdot V_m\cdot\left[\left[d_2\right]^2-\left[d_1\right]^2\right] \tag{2.43}$$

Solving for the meridional velocity ,

$$V_m=\frac{4}{\pi}\cdot\frac{Q}{\left[\left[d_2\right]^2-\left[d_1\right]^2\right]} \tag{2.44}$$

2.2.7) Type Selection of the Velocity Diagram

As mentioned before , in this study , there are no air guide vanes at the discharge of the fan . The velocity triangles are the ones as illustrated in Figure 2.6 .

2.2.8) Selection of the Number of Blades

The number of the blades generally varies from 4 to 8 . The limits lie between 2 and 50 blades [12] . If the number of blades is low (e.g. 2) the chord length and the axial chord will be too large and the guidance of the flow will be poor . On the contrary , when the number of the blades is high (e.g. 50) the chord length and the axial chord will be too small . The high number of blades also increases the losses . Moreover , the mounting of the high number of blades on the hub creates difficulties in the manufacturing of the fan . In this study , the number of the blades is selected as 8 .

2.2.9) Calculation of the Power Required to Drive the Fan

The power required to drive the fan , IP , is calculated by using Equation (2.42) . Solving for IP ,

$$IP=\frac{Q}{\eta_{tot}}\cdot\Delta p_t \tag{2.45}$$

2.2.10) Calculation of Velocities , Angles , Blade Dimensions and Blade Orientations

Considering the total efficiency in Equation (2.20) and solving for V_θ which is equal to $V_{\theta 2}$ (since $V_{\theta 1}$ is equal to zero) , one can get ,

$$V_\theta = \frac{1}{\rho \cdot U \cdot \eta_{tot}} \cdot \Delta p_t \qquad (2.46)$$

At this point , the following design calculations are performed for each value of the specified diameter . The first one being the outer diameter , while the last one being the inside diameter . These calculations are performed in order to obtain the blade shape . An alternative selection is shown in Figure 2.13 .

a) Calculations for $d = d_2$ (Outside diameter)

The following design calculation steps should be performed for the outside diameter :

i) Calculation of U

As it is known ,

$$U = \pi \cdot d \cdot N \qquad (2.47)$$

where N is the rotational speed in revolutions per second .

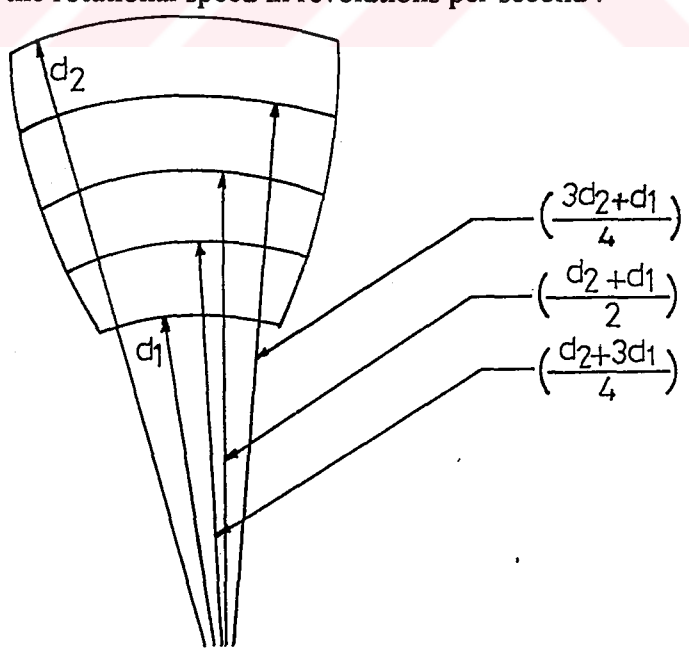

Figure 2.13 An alternative selection for the design calculations

ii) Calculation of V_θ

Using Equation (2.46) ,

$$V_\theta = \frac{1}{\rho \cdot U \cdot \eta_{tot}} \cdot \Delta p_t \tag{2.46}$$

iii) Calculation of the relative flow angle at the outlet , β_2

From Figure 2.6,

$$\beta_2 = \arctan\left[\frac{V_m}{U - V_\theta}\right] \tag{2.48}$$

iv) Calculation of the relative flow angle at the inlet , β_1

From Figure 2.6 ,

$$\beta_1 = \arctan\left[\frac{V_m}{U}\right] \tag{2.49}$$

v) Calculation of the angle of mean velocity β_∞, and the mean of the relative flow angles, β_m

$$\beta_\infty = \operatorname{arccot}\left[\frac{\cot \beta_1}{2} + \frac{\cot \beta_2}{2}\right] \tag{2.50}$$

$$\beta_m = \frac{[\beta_1 + \beta_2]}{2} \tag{2.51}$$

vi) Calculation of the pitch , t

$$t = \pi \cdot \frac{d}{Z} \tag{2.52}$$

vii) Calculation of the ratio of the pitch to the chord length of the blade

The t / ℓ ratio can be calculated by solving Equation (2.36) for t / ℓ,

$$\frac{t}{l}=\frac{C_L \cdot \rho \cdot U \cdot V_m \cdot \eta_{tot}}{2 \cdot \sin[\beta_\infty] \cdot \Delta p_t} \tag{2.53}$$

There are some well known profiles for propeller fans in practice . For instance , Gottingen profiles no 682 , 622 , 623 . Generally , for most of the profiles , the lift coefficient is selected in the range where the drag coefficient is minimum . As an average C_L = 0.5 - 0.6 can be chosen [13] . In this study , C_L is chosen as 0.6 . Also in practice , the best values of t / ℓ lie in the range $0.5 < t / \ell < 1.5$ [13] .

$$l=\frac{t}{\left[\frac{t}{l}\right]} \tag{2.54}$$

viii) Calculation of the Overall Deflection of the Flow

The overall deflection of the flow is the turning of relative flow across the impeller and defined as ,

$$\nu_\infty=\beta_2-\beta_1 \tag{2.55}$$

ix) Calculation of Excessive Bending , μ

In order to deflect the relative flow by the required amount i.e, ν_∞, the circular arc should have a bending larger than overall deflection . The excessive bending μ is the ratio of overall deflection to blade turning . According to Weinig [14] , an excessive bending is selected in such a way that circular arc blades with a deflection of $\nu > \nu_\infty$ are determined . $\mu = \nu_\infty / \nu$ is obtained from experimental results shown in Figure 2.14 with the known t / ℓ and β_m values .

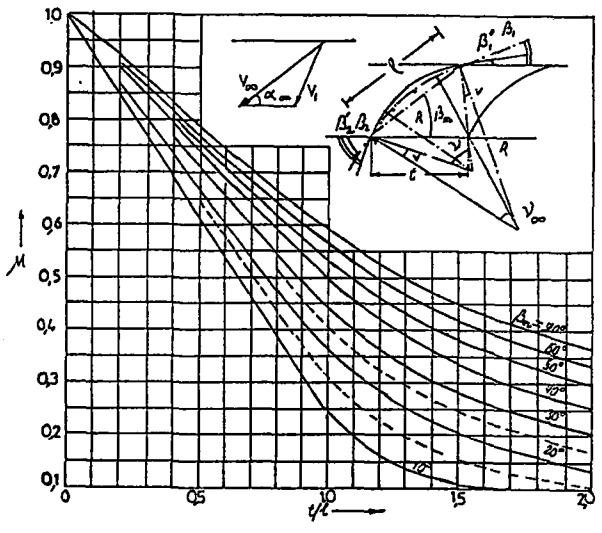

Figure 2.14 Cascade calculation according to Weinig [14]

x) Calculation of Local Excess , v

Weinig [14] states that local excess is equal to

$$v=\frac{\left[\nu-\nu_{\infty}\right]}{2}=\frac{\nu_{\infty}}{2}\cdot\frac{(1-\mu)}{\mu} \qquad (2.56)$$

Different autorities recommend that all of the excess curvature can be given to the blade outlet . There can be no excess curvature given to the blade inlet [13] .

xi) Calculations of Blade Angles $\beta_{1'}$ and $\beta_{2'}$

The blade angles $\beta_{1'}$ and $\beta_{2'}$ are expressed in a cascade as shown in Figure 2.15 .

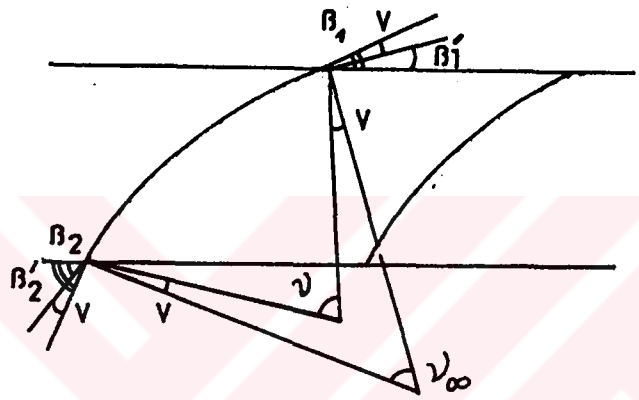

Figure 2.15 Blade angles in a cascade

From Figure 2.15 ,

$$\beta_{1'}=\beta_1-v \qquad (2.57)$$

$$\beta_{2'}=\beta_2+v \qquad (2.58)$$

xii) Calculation of the Ultimate Opening Angle , $\Delta\beta$

Shemoyama [15] has found that at the inlet an increase in v_{∞} occurs in the flow through the cascades of the aerofoils . A correction which depends on the thickness , chord length , mean of the relative flow angles and pitch is determined according to the following formula :

$$\Delta\beta=\Delta\beta_1\cdot\left[\frac{l}{t}\right]^2 \qquad (2.59)$$

where $\Delta\beta_1$ value is found from Figure 2.16 which is experimentally obtained .

Note that s / ℓ is the ratio of maximum blade thickness to the chord length , and is generally selected as 0.06 at the tip and 0.065 at the hub [16] . In this study , the blade thickness , s is considered as constant throughout the cross-section and s / ℓ is selected as 0.06 at all radii .

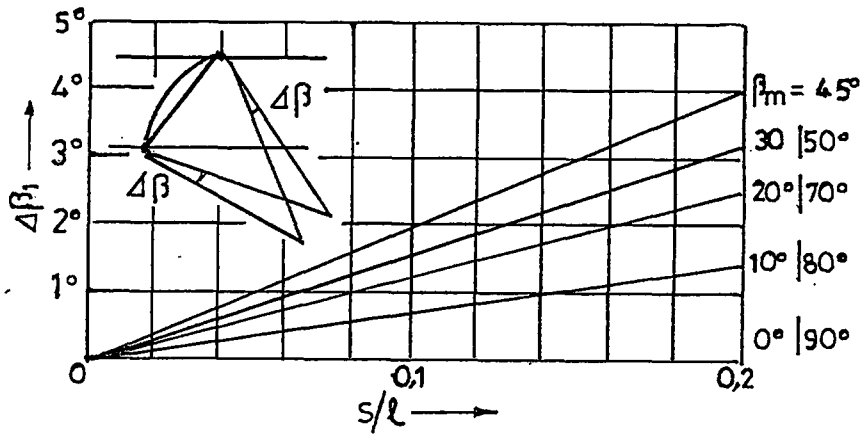

Figure 2.16 Chart for determining the increase of angle by profiling [15]

xiii) Calculation of Corrected Blade Angles , $\beta_{1''}$, $\beta_{2''}$ and the stagger angle , $\beta_{m''}$

The corrections on the blade angles can be carried out by the following calculations :

$$\beta_{1''}=\beta_{1'}+\Delta\beta \qquad (2.60)$$

$$\beta_{2''}=\beta_{2'}+\Delta\beta \qquad (2.61)$$

$$\beta_{m''}=\beta_{m}+\Delta\beta \qquad (2.62)$$

xiv) Determination of the Geometry of the Blade

The relations between the angles , the radius of curvature R and the chord length of the cascade of a circular arc blade are summarized below as shown in Figure 2.17.

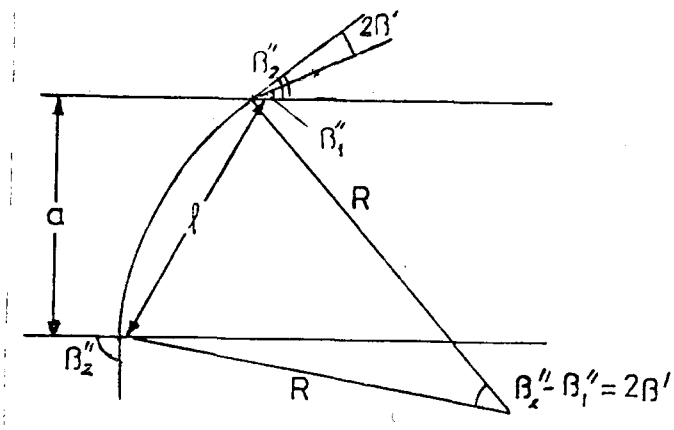

Figure 2.17 Geometry of the blade

$$\beta' = \frac{\left[\beta_{2''} - \beta_{1''}\right]}{2} \tag{2.63}$$

$$R = \frac{l}{2 \cdot \beta'} \tag{2.64}$$

$$a = R \cdot \left[\cos \beta_{1''} - \cos \beta_{2''}\right] \tag{2.65}$$

xv) Calculation of the Blade Thickness , s

The blade thickness is calculated simply as ,

$$s = \frac{s}{l} \cdot l \tag{2.66}$$

b) Calculation for Another Diameter

The design steps from (i) to (xv) have to be performed for a specified diameter which is less than the outside diameter . The procedure is ended when the inside diameter is reached . The complete blade shape is obtained by using the following way·

The cross-sections of the blades at selected radii are put on each other so that the mid-point of the chord length of each blade passes through the same point .

As a conclusion , after the design procedure the shapes of the blades at different diameters are shown in Figure 2.18 .

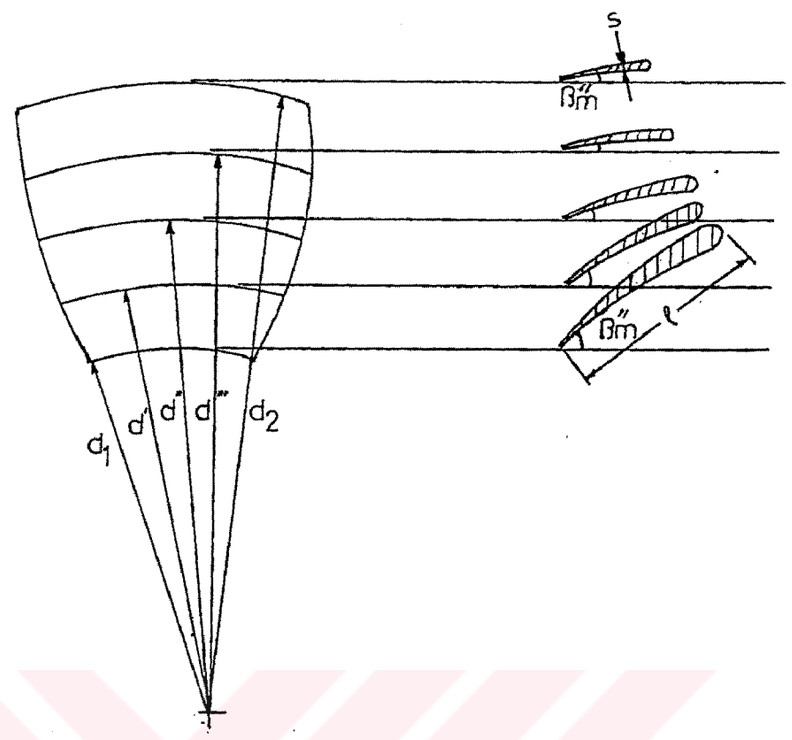

Figure 2.18 Blade shape and orientation after the design steps are applied

2.2.11 Strength Calculation of the Axial Fan

It is important that some attention has to be paid to the stressing of impellers by centrifugal forces during the design procedure . One can consider all blades of the axial fans as rotating bars or spoke-shaped configurations . Knowing this situation , one can imagine a freely rotating bar as shown in Figure 2.19 .

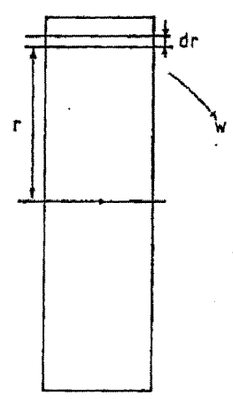

Figure 2.19 Freely rotating bar

Consider a bar of constant cross-section f is rotating at the peripheral speed U as shown in Figure 2.19 . The centrifugal force acting on an infinitessimal thickness of dr ,

$$dF_c = dr \cdot f \cdot \frac{\rho_m}{g} \cdot r \cdot w^2 \tag{2.67}$$

where F_c is the centrifugal force in Newtons , f is the cross-sectional area of the bar in meter square , ρ_m is the density of the material of the bar in kilograms per meter cube , r is the radius in meters , w is the rotational speed in revolutions per second and g is the gravitational acceleration in meters per second square .

When Equation (2.67) is integrated from r_1 to r_2 ,

$$F_c = f \cdot \frac{\rho_m}{g} \cdot \frac{\left[[U_2]^2 - [U_1]^2 \right]}{2} \tag{2.68}$$

The centrifugal force F_c causes a tensile stress Ω which has the highest value at the middle of the bar , that is , for r is equal to zero [17]. This stress in the cross-section is equal to ,

$$\Omega = \frac{F_c}{f} \tag{2.69}$$

also using Equation (2.69) ,

$$\frac{F_c}{f} = \frac{\rho_m}{2g} \cdot \left[1 - \left[\frac{r_1}{r_2} \right]^2 \right] \cdot [U_2]^2 \tag{2.70}$$

Equating both Equations (2.69) and (2.70) , one may reach ,

$$\Omega = \frac{\rho_m}{2g} \cdot [U_2]^2 \quad \text{for } r_1 = 0 \tag{2.71}$$

According to Equation (2.71) , the tensile stress is only a function of the peripheral velocity . At this point , the rotating bar can be compared to the axial fan blade . Therefore , a non-dimensional parameter , k can be introduced as follows :

$$k = \frac{\Omega_{max}}{\left[\frac{\rho_m}{2g} \right] \cdot [U_2]^2} \tag{2.72}$$

From Equation (2.72) ,

$$\Omega_{max}=\frac{\rho_m}{2\cdot g}\cdot k\cdot\left[U_2\right]^2 \tag{2.73}$$

The non-dimensional parameter parameter , k explains how many times that the largest tensile stress acting in an impeller is greater compared to the tensile stress acting in a rotating bar . All parameters on the right hand side of Equation (2.73) except k are known previously . The non-dimensional parameter k can be found from the chart arranged experimentally as shown in Figure 2.20 . With the known dimensions of the axial fan blade , the corresponding k value of the axial fan blade is found from Figure 2.20 .

Considering the safety factor , the allowable stress according to design becomes ,

$$\Omega_{design}=\Omega_{max}\cdot n \tag{2.74}$$

where n is the safety factor . The safety factor considered in the axial fan design procedures ranges between 2.5 and 3.5 [17] . As it is known , the design stress has to be smaller than the tensile yield strength of the material used in the manufacturing of the axial fan .

In Figures 2.21 to 2.24 , the top view and side view of the designed axial fan , cross-sectional view of a blade on the hub and orientation of the blade sections at selected radii are shown . The design steps from (i) to (xv) are performed for ten diameters as shown in Figure 2.24 . The outer circle corresponds to the outside diameter , whereas , the inner circle corresponds to the inside diameter of the fan . On the top of the figure , the chord length of the blades and corresponding stagger angles at each diameters are illustrated . These figures are obtained from the computer output . The flow chart of the design procedure is illustrated in Figure 2.25 .

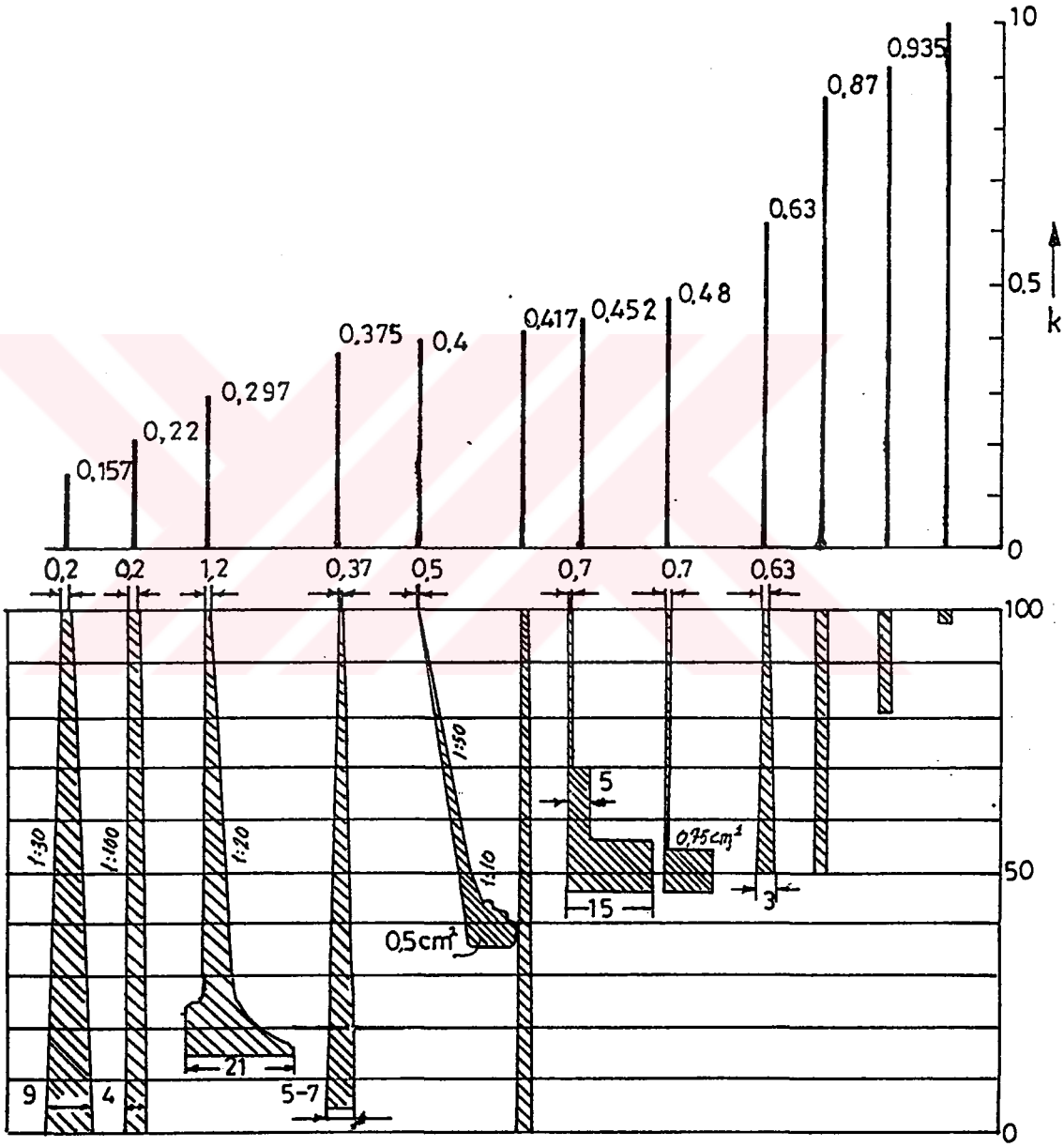

Figure 2.20 Stress properties of typical impellers shown as dimensionless ratios [17]

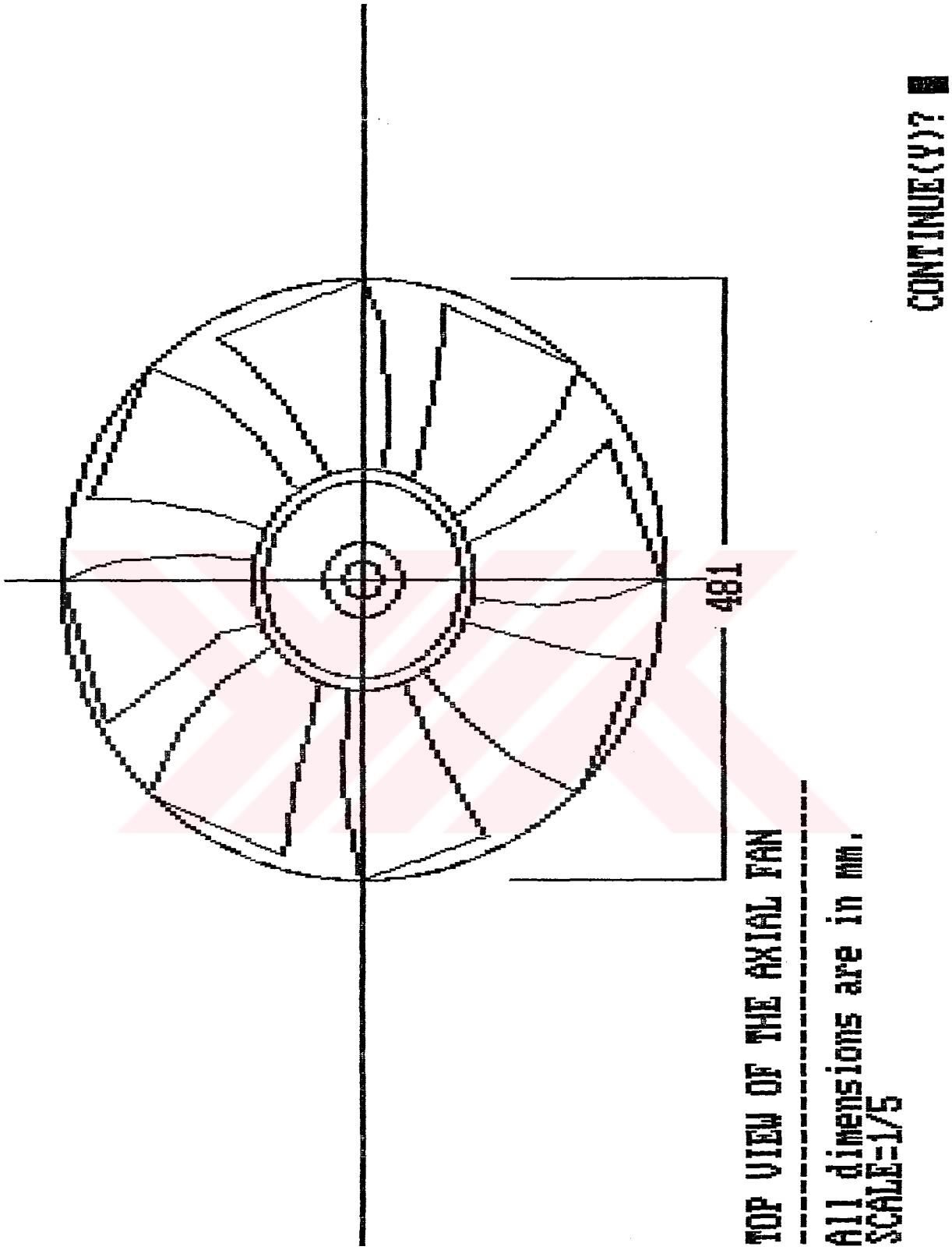

Figure 2.21 Top view of the axial fan

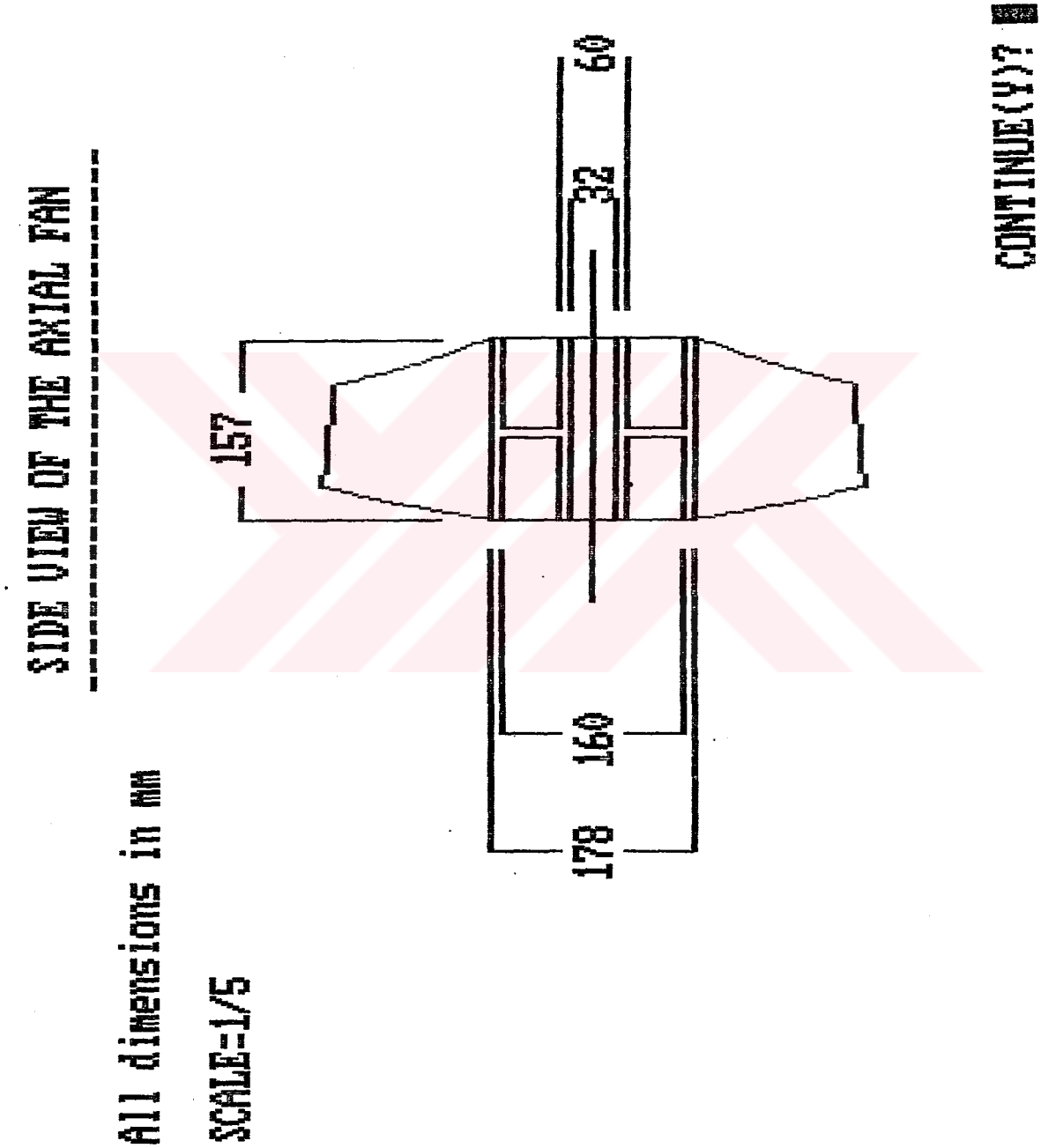

Figure 2.22 Side view of the axial fan

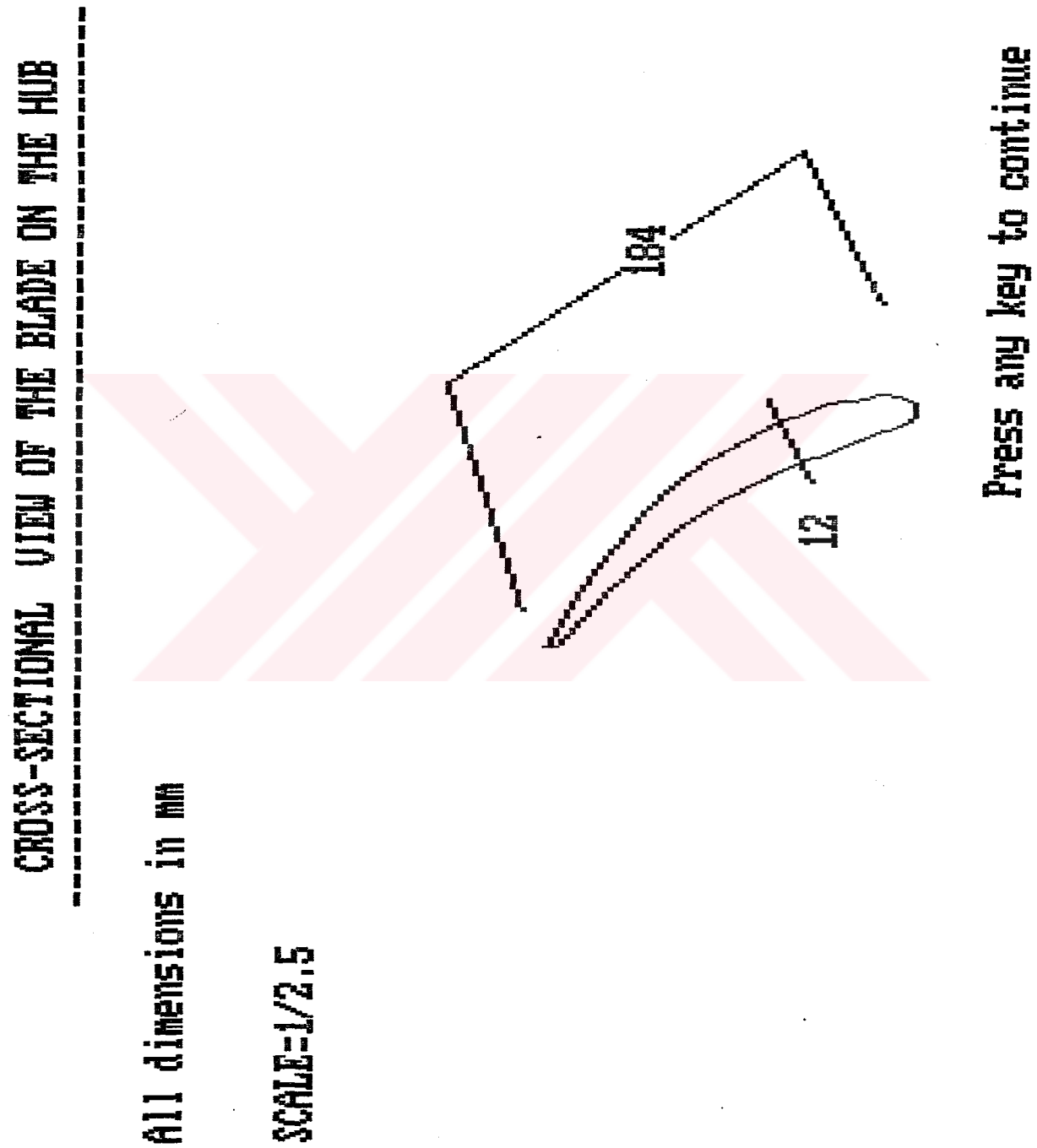

Figure 2.23 Cross-sectional view of the blade on the hub

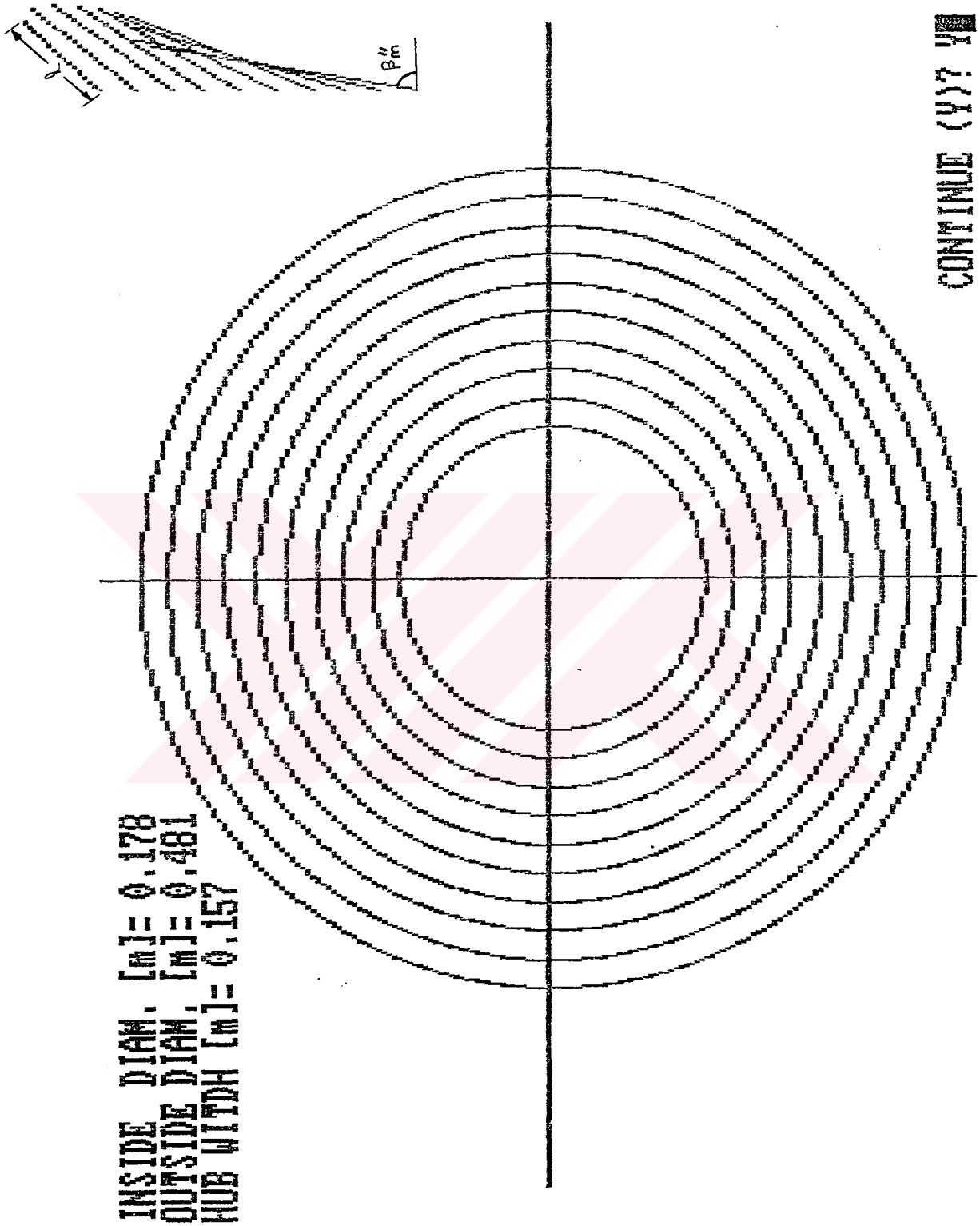

Figure 2.24 Orientation of the blade sections at selected radii

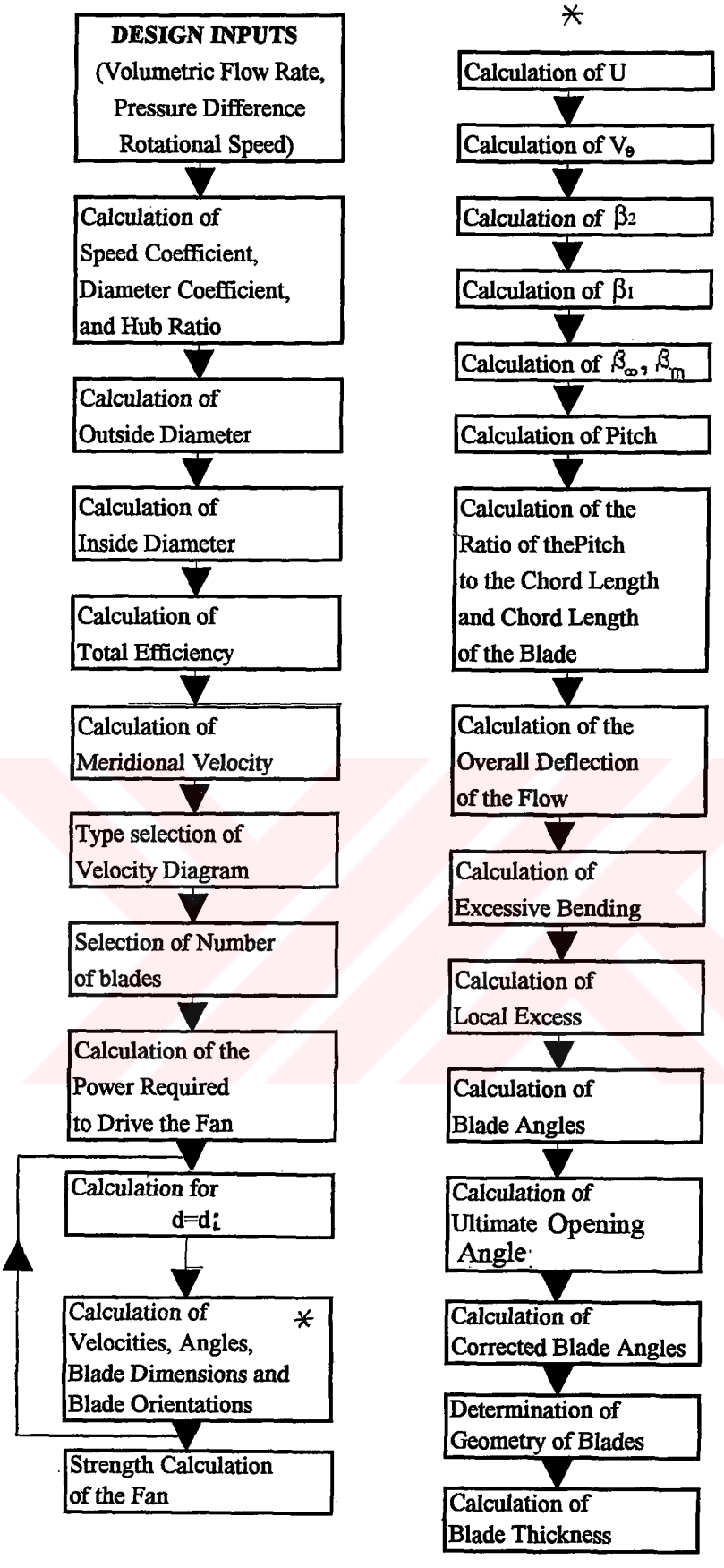

Figure 2.25 Flowchart of the design procedure

CHAPTER III

MANUFACTURING

At this point , the axial fan is ready to be manufactured since all of the parameters required for the manufacturing of the fan are determined previously in Chapter II . The manufacturing of the fan is carried out in three steps :

i) Making the model of the fan ,
ii) Sand casting of the fan and
iii) Turning operations .

3.1 Model of the fan

It is obvious that the most important part of the manufacturing of the axial fan is making the model of the fan . Unless one obtains a precise and accurate model of the fan , he or she can never get good results from the sand casting process . The model is a duplicate of the fan which is to be casted. As it is known , the material of the model is determined primarily by the number of the castings to be made . Wood models are relatively easy to make and are usually utilized when a small number of castings are needed . However , wood models are not very stable dimensionally , therefore they can change their dimensions with changes in the humidity . On the other hand , metal models are relatively more expensive , but are more stable dimensionally . Also , they can be used for a longer period of time . In this study , in order to make the model of the axial fan both wood and metal are used . The hub of the axial fan is modelled by using wood , on the contrary , the models of the blades of the fan are made by Aluminum . The reason that Aluminum is used for eight blades is just for duplicating the blade profile which is made by wood . After the model of the hub of the fan is obtained , then eight Aluminum blades are mounted on it in a very strong manner to have the complete model of the fan . The photograph of the model of the axial fan is shown in Figure 3.1 .

Therefore , modelling of the fan can be also considered in two phases:

i) Making the model of the hub
ii) Making the models of the blades

When making the model of the hub of the fan , wood materials are shaped according to hub dimensions which are previously determined . In particular , it is easy to make the hub model when compared with the blades . The wooden model of the hub are made by joining four equally divided portions . The mounting operations are achieved by using special glue having a high bonding strength . Finally , the model is covered by a steel paste and completely painted .

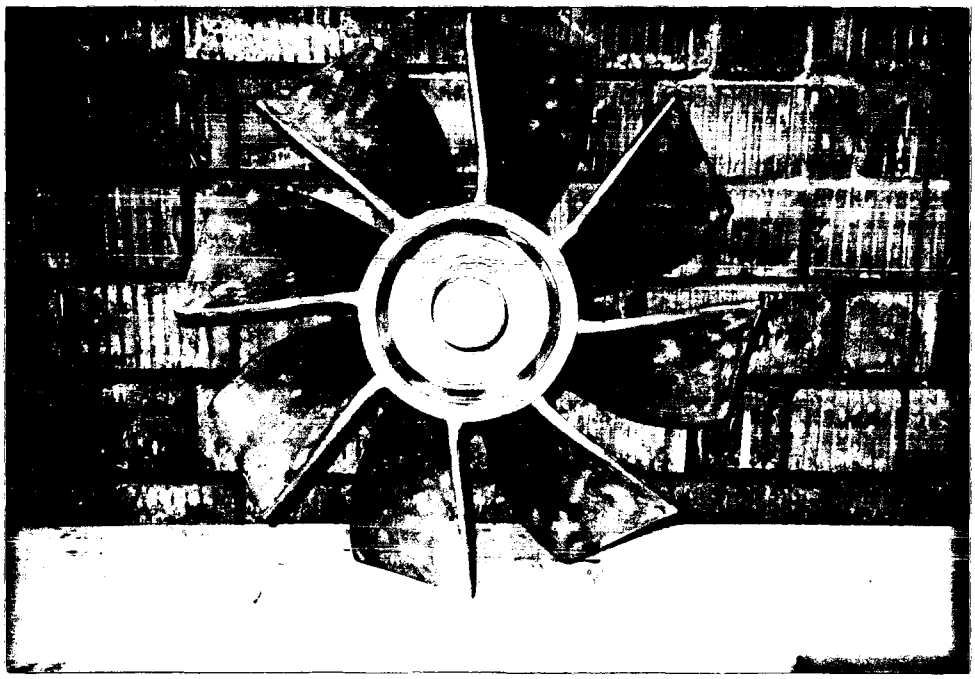

Figure 3.1 The model of the axial fan

It should be noted that the manufacturing of the models of the blades is a difficult operation . Firstly , the calculated blade height is divided into ten equal portions . Thus , each divisions corresponds to a different outside diameter . Also, the blade angle and blade length for these divisions are known since they are calculated in Chapter II . Then , the blade figures of the ten divisions are drawn on different cartoon plates . The drawings are made in full scale . These drawings are shown in Figure 3.2 .

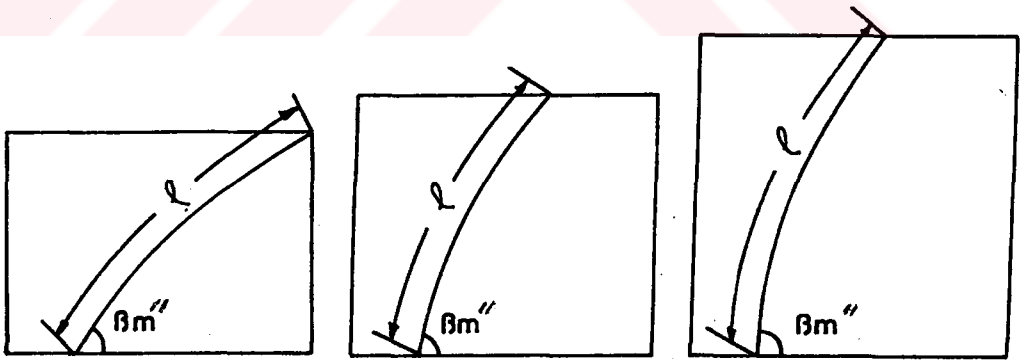

a) Division 1
At the tip

b) Division 5
At the middle

c) Division 10
At the hub

Figure 3.2 The sketch of blades at different divisions

Figure 3.1 The model of the axial fan

It should be noted that the manufacturing of the models of the blades is a difficult operation . Firstly , the calculated blade height is divided into ten equal portions . Thus , each divisions corresponds to a different outside diameter . Also, the blade angle and blade length for these divisions are known since they are calculated in Chapter II . Then , the blade figures of the ten divisions are drawn on different cartoon plates . The drawings are made in full scale . These drawings are shown in Figure 3.2 .

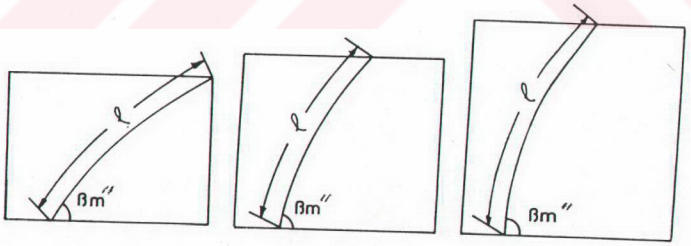

a) Division 1
At the tip

b) Division 5
At the middle

c) Division 10
At the hub

Figure 3.2 The sketch of blades at different divisions

Then , the blade figures are removed from the cartoon blades by cutting them through the curves designating the blade length . Figure 3.3 shows a blade figure for one division .

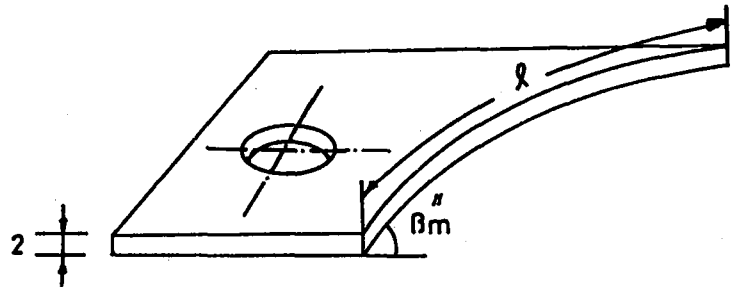

Figure 3.3 A blade figure for one division

As the next operation , steel plate having a thickness of 5 millimeters and a steel bar having a diameter of 10 millimeters are used for the construction of the base shown in Figure 3.4 .

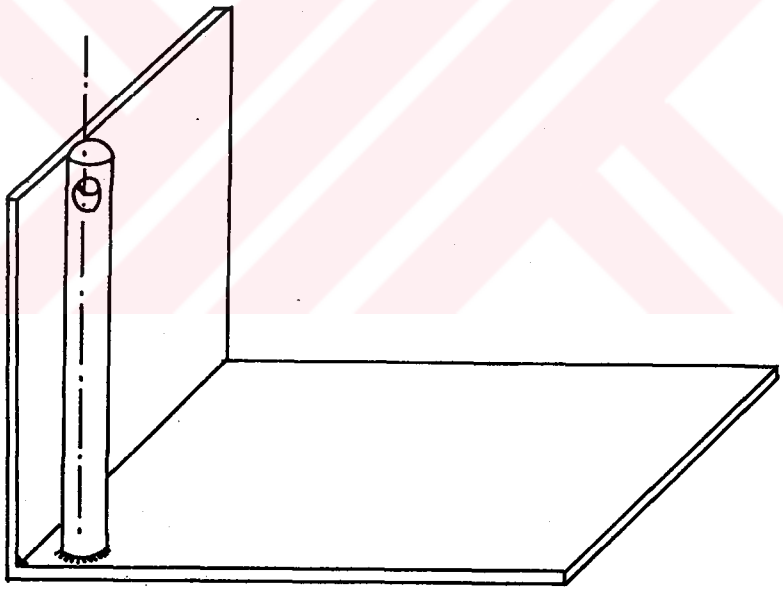

Figure 3.4 The base onwhich the divisions are mounted

Then the divisions are placed on the base by putting one on top of the other . Small and thin plates are placed between the divisions to have the exact blade height . This arrangement is shown in Figure 3.5 . Owing to different blade lengths and angles at differtent divisions , a cavity appears on this arrangement . This cavity is the blade cavity or in other words blade profile .

Next , a rectangular prism made of gypsum is provided . Then , this prism is placed on the base of the arrangement . Then , the prism is moved towards

to the mounted divisions . Thus , the gypsum prism is touched to the ten divisions which create the blade cavity or profile . Then , the touching side of the prism is

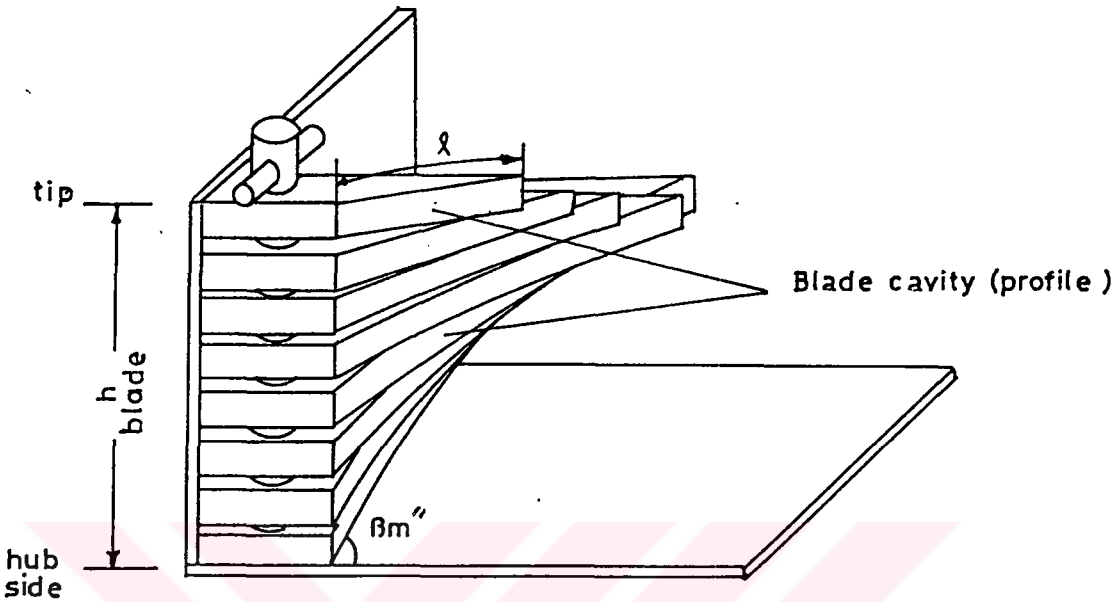

Figure 3.5 The arrangement for making a blade model

shaped according to the blade profile by removing small pieces of gypsum material . Sharp cutting devices and small grinders are used to shape the gypsum prism . At this moment , the blade profile is copied from the arrangement to the gypsum prism . At this step ,the objective is to copy this profile on to the model which is made of wood . Similarly ,a wooden block is machined to get the blade profile .Cutting and hand grinding operations are done to have the blade profile on the wood model . Thus , the copy of the blade profile is obtained on the wood . Since the blade thicknesses at the ten divisions are known , the wooden model is made by applying the thicknesses at each of the divisions. The blade profile is the same on both sides of the model . The thickness and blade length of the model are in their maximum values at the hub side and they are in their minumum values at the tip side . The thickness and the length of the blade model decrease gradually from the hub to the tip . Therefore , the wooden model of a blade is obtained . Now , this wooden model is placed on the bottom piece of the mold (1) filled with sand as shown in Figure 3.6 a . The force is exerted on the top of the model until the half of the model penetrates into the sand mold . A powder like material is spreaded on the bottom piece of the mold so as to have a parting line between the two pieces of the mold . Then , the top piece of the mold (2) which is empty at this moment is placed on the bottom piece (1). Two bars called a sprue and a riser are placed near the model in the vertical direction . Next , the top piece of the mold is filled with sand and squeezed by applying impact forces on the top of the mold . This is shown in Figure 3.6 b. Then , the mold is opened and the model , the sprue

and the riser are removed from the mold as shown in Figure 3.6 c . Also at this step , in the bottom piece of the mold , a small cavity is made near the model . This cavity is called the runner and the gate . Next , the mold is closed . There are two holes namely a sprue and a riser hole in the top piece of the mold . Molten Aluminum is poured into the sprue hole and enters the runner and gate and finally fills the profile of the blade . The rate of the molten Aluminum flow is controlled by the riser hole . This step is shown in Figure 3.6 d . After the solidification of Aluminum in the mold , the sand mold is broken and the casting of the blade profile is removed from the mold . The castings of the sprue , the riser, the gate and the runner are also attached on the casting of the blade , as shown in Figure 3.6 e . The castings of the sprue , the riser , the gate and the runner are removed from the casting of the blade .

The sand casting process explained in the previous paragraph is repeated eight times to get the models for eight blades . These casted blades are surface finished and covered with steel paste to achieve an improvement in surface quality of the models .

As a consequence , eight blades are mounted on the hub by grooving eight equally spaced canals on the hub and assembling the blades in these canals . Furthermore , the model of the fan is made slightly larger than the desired casting due to the consideration of shrinkage allowance . When the typical allowances of 1.0 - 1.3 % for Aluminum [18] are taken into account , the model dimensions are considered as approximately 1.0 % larger than the required dimensions . Also , an allowance for the finishing operation is provided on the model of the fan .

3.2 Sand Casting of the Fan

Since the model of the fan is ready , the next step is the sand casting of the axial fan . The casting procedure is exactly same as the procedures for making the models of the blades . Firstly , the model of the fan is placed in the bottom piece of the sand mold which is filled with squeezed sand . Then , the cavity of the half of the fan is obtained in the sand by exerting a force on the top . Next , the riser and the sprue are placed and a powder like material is spreaded to have a parting line . Then , the top of the mold is placed on the bottom piece and filled ith sand . The sand is squeezed by exerting impact forces on the top . After this, the mold is opened and the model of the fan , the sprue and the riser are removed . A gate and a runner are made in the bottom piece of the mold . Then , the mold is closed and molten Aluminum is poured into the sprue hole . After the solidification of Aluminum in the mold , the mold is broken and the casting of the axial fan is removed . The time between pouring of the molten Aluminum and breaking the mold to remove the casting is nearly twelve hours . The runner , the gate , the sprue and the riser are also removed from the casting of the fan .

It is remarkable that the preperation of the model ofthe axial fan takes about 120 hours and the sand casting takes nearly 24 hours . This work is completed by one qualified technician .

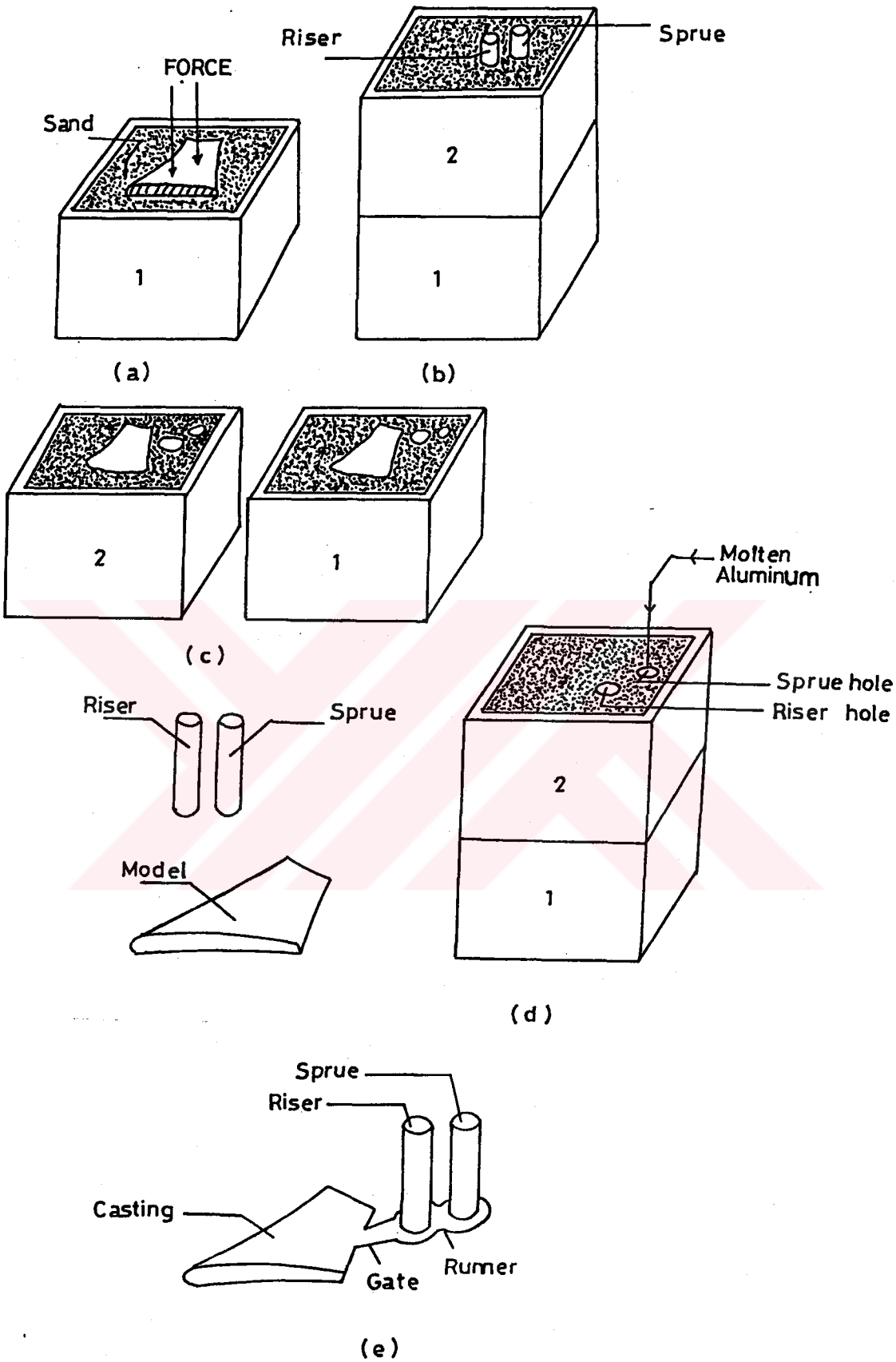

Figure 3.6 Sand casting operations for making blade models

3.3 Turning Operations

When the cast of the axial fan is removed by breaking the sand mold , it has some irregularities and dimensional differences in the desired design parameters . For instance , the outer diameter of the fan is approximately 15 millimeters larger than the model and the surface quality of inside of the hub is not perfect . In order to eliminate these effects , turning and boring operations are performed by using a universal lathe . The inner side of the hub is machined to get a good surface quality . Indeed , the outer diameter of the fan is decreased to the desired value by turning . This lathe operation on the outer diameter provides an accurate circular shape which was poor after casting . Furthermore , boring operations on the same lathe are used to determine the shaft hole and key way on the hub of the fan . The irregularities between the blades are small in size and they are eliminated by hand grinding operations .

CHAPTER IV

PERFORMANCE EVALUATION

The performance evaluation of the manufactured axial fan is done in two phases :

1) Construction of the test set-up
2) Making performance tests

4.1 Construction of the Test Set-up

As it is mentioned before , the performance evaluation of the manufactured fan is carried out according to ASHRAE (American Society of Heating , Refrigerating and Air Conditioning Engineers) Standard 51-75 . The drawing of the experimental set-up according to ASHRAE Standard 51-75 is illustrated in Figure 4.1 .

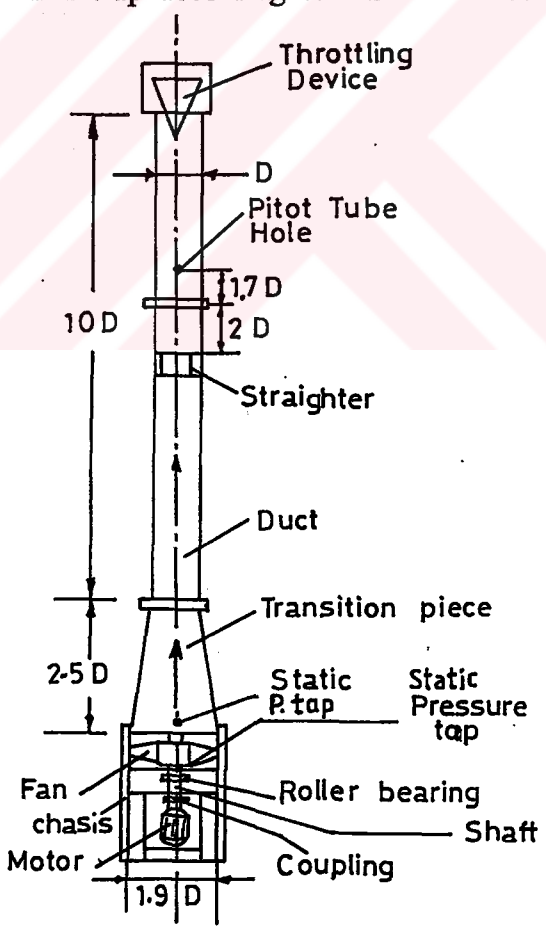

Figure 4.1 The experimental set-up for performance tests

It should be stated that the connection of the axial fan to the set-up is relatively difficult compared to building the set-up the connection between the axial fan shaft and the electric motor shaft is done by using a coupling . Two roller bearings with their housings are placed on the fan shaft and the housings are mounted on chasis of the fan . The chasis is designed and manufactured with the consideration of minimum losses in the air inlet conditions . Generally , U and L steel profiles are cut and welded together for constructing the chasis .

Before the axial fan is mounted on the set-up , the fan is balanced by the use of a special fan balancing machine . Then , the fan is mounted on the shaft and then the axial fan is mounted on the chasis by using two roller bearings and housings . After these operations are performed , the connection between the shaft of the fan and shaft of the electric motor is done by a coupling . The connection should be done in a precise manner in order to eliminate undesired stress on the motor and the shaft .

As it can be seen from Figure 4.1 , the duct which is made by rolling steel with plates with a thickness of 1 millimeter is connected to the casing of the fan by using a transition piece . A flow straightner is placed in the duct to have uniform flow conditions . A throttling device having a cone shape is used to achieve the throttling of the flow . This device is for obtaining the off-design operating points in the performance tests . In order to minimize the air leakage between the connections , all of the connections on the apparatus relavant to the air flow are wrapped by using a strong insulating tape . The photograph of the experimental set-up for performance evaluation is shown in Figure 4.2 .

Figure 4.2 The photograph of the set-up

4.2 Making Performance Tests

When the construction of the set-up is completed , the performance tests are carried . The following parameters are considered as fan performance variablies :

i) Flow rate
ii) Total pressure increase
iii) Dynamic pressure increase
iv) Static pressure increase
v) Power output
vi) Total efficiency
vii) Total head
viii) Dynamic head
ix) Static head

When making performance tests , the above parameters are obtained for each different operating point corresponding to a particular flow rate on the fan characteristic curve . The operating points are controlled during the test by adjusting the position of the throttling device mounted at the outlet part of the apparatus . In the performance evaluation of the fan , five different operating points are utilized . Therefore , for each operating point all of the values of the performance variables are determined . During the performance tests , the following steps are encountered :

i) Determination of the static , dynamic and total pressure increases across the fan

The determination of the static pressure rise across the fan is achieved by the measurement of the pressure difference between the inlet and outlet of the fan by using an inclined manometer . Because of the small pressure difference , an inclined manometer with alcohol is used . The connection of the manometer to the apparatus is schematically shown in Figure 4.3 .

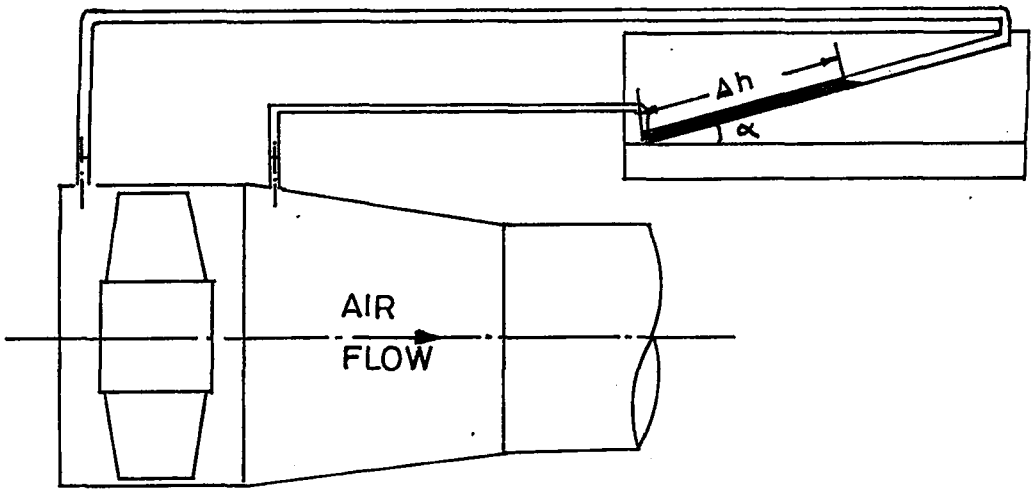

Figure 4.3 The inclined manometer connection to the apparatus

The deflection of the inclined manometer column gives the static pressure increase across the axial fan in terms of the meters of alcohol as it can be seen from Figure 4.3. The static pressure rise can be easily calculated by using the following formula :

$$\Delta p_{stat} = \rho \cdot g \cdot \sin(\alpha) \cdot \Delta h \qquad (4.1)$$

where Δh is the deflection in the inclined manometer in meters , ρ is the density of alcohol in kilograms per cubic meters , g is the gravitational acceleration in meters per second square and α is the angle of the inclined manometer .

In order to determine the dynamic pressure increase across the fan , a Pitot tube is used . The Pitot tube traverse locations are illustrated in Figure 4.4 . The static pressure leg of the Pitot tube is connected to the upper end of the inclined manometer , whereas the total pressure leg is connected to the lower end of the manometer as shown in Figure 4.5 . Since the total pressure is normally greater than the static pressure , the fluid in the manometer rises in the upward direction . Thus , the deflection in the manometer gives the dynamic pressure increase in terms of meters of alcohol . And Equation 4.1 can be used to calculate the dynamic pressure difference across the fan at each of the Pitot tube traverse points . To find an average value for the dynamic pressure , the following formula can be used :

$$\Delta p_{dyn} = (\Delta p_{dyn})_{ave} = \frac{\left[\sum \sqrt{\Delta p_{dyn}}\right]^2}{n^2} \qquad (4.2)$$

In the above equation , the square roots of the dynamic pressure values at all of the Pitot tube traverse points are summed and this summation is divided to the number of points , n .

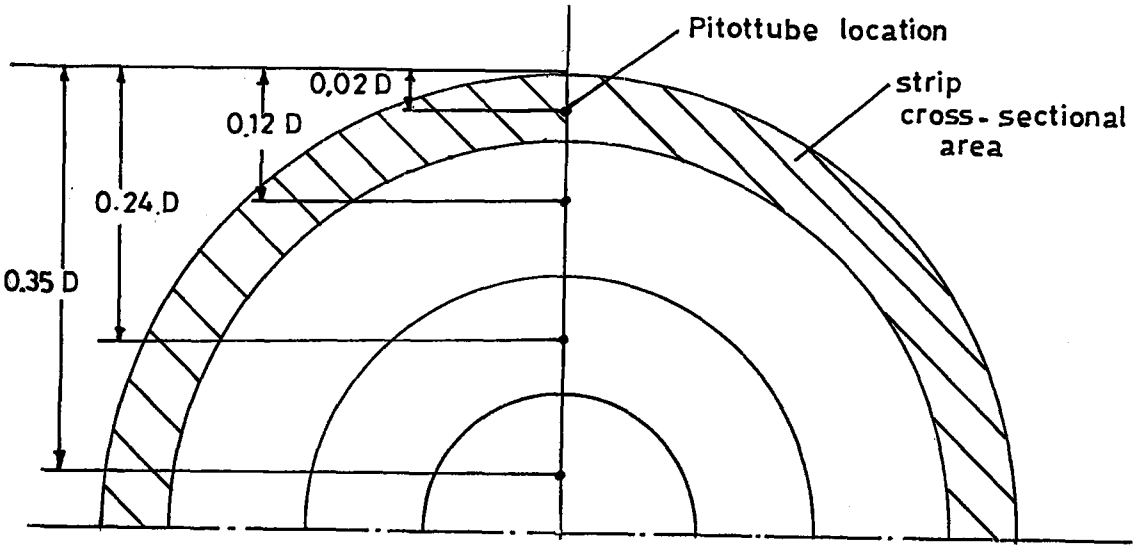

Figure 4.4 Pitot tube traverse locations in the duct

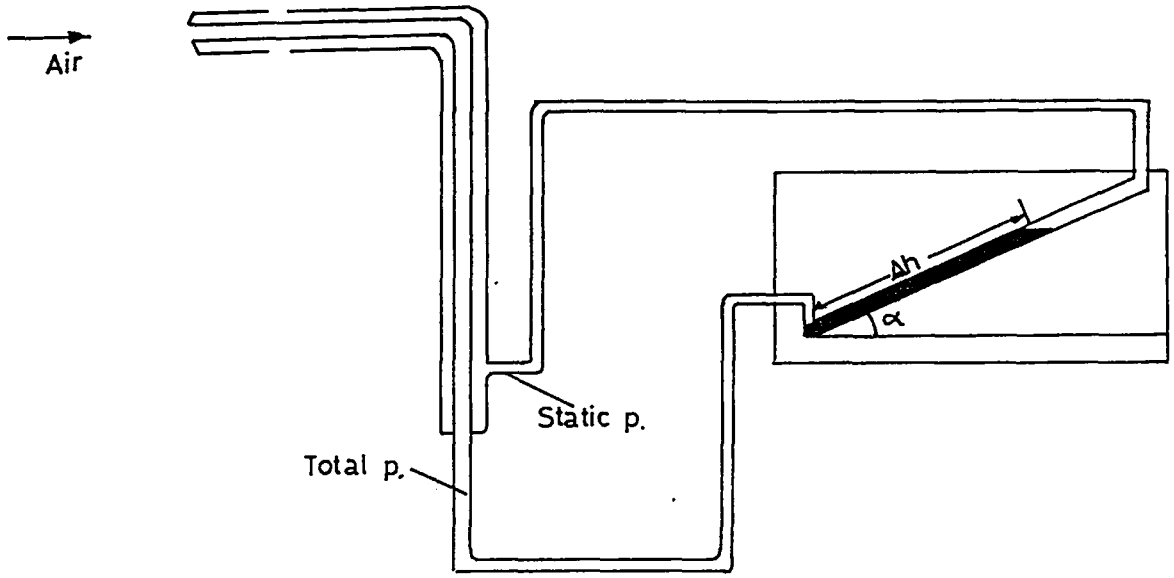

Figure 4.5 Pitot tube connected to the inclined manometer

The total pressure increase of the axial fan is simply calculated by adding the static and dynamic pressure increases . Therefore ,

$$\Delta p = \Delta p_{tot} = \Delta p_{stat} + \Delta p_{dyn} \qquad (4.3)$$

Since the static , dynamic , and therefore total pressure increase of the axial fan are calculated at this step , it is easy to determine the static head , dynamic head and the total head delivered by the fan by using the following relations :

$$H_{stat} = \frac{1}{\rho \cdot g} \cdot \Delta p_{stat} \qquad (4.4)$$

$$H_{stat} = \frac{1}{\rho \cdot g} \cdot \Delta p_{dyn} \qquad (4.5)$$

$$H = H_{total} = \frac{1}{\rho \cdot g} \cdot \Delta p \qquad (4.6)$$

where ρ is the density of water in kilograms per cubic meter .

ii) Determination of the volumetric flow rate delivered by the fan

To calculate the volumetric flow rate Q created by the axial fan , the Pitot tube arrangement same as step i can be used for determining the velocity of the flow . If one writes the Bernoulli Equation between points 1 and 2 as illustrated in Figure 4.6 , the following equation will be obtained :

The velocity at point 2 is zero ,

$$V_1 = V = \sqrt{2 \cdot g \cdot \left[\frac{\rho_{alc}}{\rho_a} - 1\right] \cdot \sin(\alpha) \cdot \Delta h} \qquad (4.7)$$

In the above equation , ρ_{alc} is the density of alcohol in kilograms per cubic meter , ρ_a is the density of air in kilograms per cubic meter , V is the velocity at point 1 in meters per second and Δh is the deflection of the inclined manometer at a specific Pitot tube traverse point , in meters .

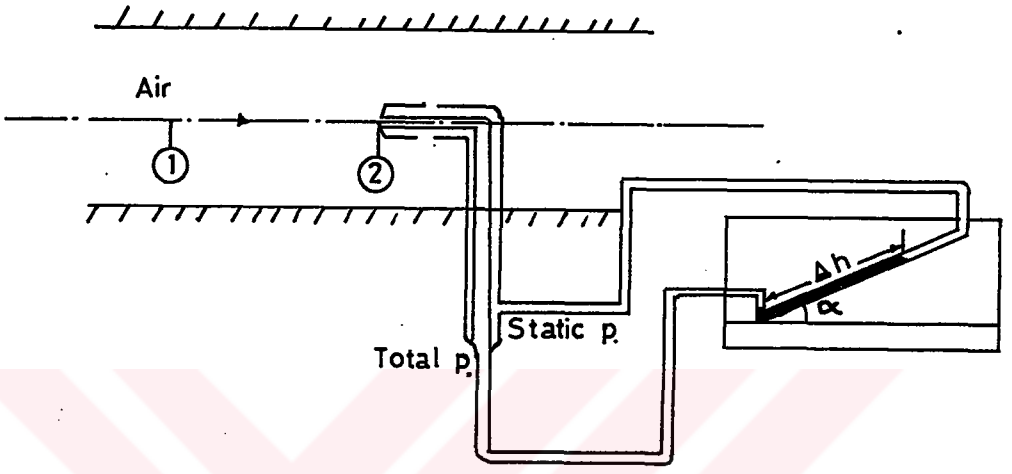

Figure 4.6 Pitot tube placed in the air flow

The volumetric flow rate Q is calculated by using the following equation :

$$Q = V_1 \cdot A_1 + V_2 \cdot A_2 + V_3 \cdot A_3 + V_4 \cdot A_4 \qquad (4.8)$$

where V_n is the velocity of the flow at the Pitot tube traverse point n , in meters per second and A_n is the strip cros-sectional area at the Pitot tube traverse point n , in meters square .The strip cross-sectional area for a Pitot tube traverse point is also shown Figure 4.4 .

iii) Determination of the output power of the fan

The energy delivered to air by the axial fan in other words the output power of the fan can be determined by using the following equation:

$$IP_0 = \Delta p_t \cdot Q \qquad (4.9)$$

where Δp_t is the total pressure increase across the fan , in Newtons per meter square , $\dot{Q}$ is the volumetric flow rate in cubic meters per second and $\mathbb{P}_o$ is the output power of the fan , in Watts .

iv) Determination of the total efficiency

The total efficiency of the axial fan is calculated by obtaining the ratio of the output power to the power required to drive the fan . Thus ,

$$\eta_{tot} = \frac{\mathbb{P}_o}{\mathbb{P}} \tag{4.10}$$

where ,

$$\mathbb{P} = E \cdot I \cdot \cos(\phi) \tag{4.11}$$

where , E is the voltage across the electric motor and it is measured by using a voltmeter ; its unit is Volts . I is the current passing through the electric motor in Amperes and it is measured by using an Ampermeter . The constant $\cos(\phi)$ is the cosine of the phase angle of the electric motor . $\mathbb{P}$ is the power required to drive the fan , in other words power input to the fan in Watts .

CHAPTER V

RESULTS

The performance of the manufactured axial fan is evaluated by the aid of experiments . The experiments are performed mainly with two different air inlet conditions . Firstly , the performance tests are carried out by using the set-up which is located on the ground . The width of the steel plate on which the electric motor is mounted is 600 millimeters . Since this width is equal to to the chasis width , it covers a large space in front of the inlet of the fan . Thus , this wide plate is disturbing the flow at the inlet of the fan . The results obtained from these experiments are given in Table 5.1 .

Table 5.1 The results of the performance tests with poor air inlet conditions

MEASUREMENT NO		1	2	3	4	5
Static pressure inc.	Pa	220	219.3	218.3	208.2	205.6
Dynamic pressure inc.	Pa	9.5	10.2	11.1	20.8	22
Total pressure inc.	Pa	229.5	229.5	229.4	229	227.6
Static head	mmWG	22.5	22.4	22.3	21.2	21.0
Dynamic head	mmWG	0.9	1.0	1.1	2.1	2.2
Total head	mmWG	23.4	23.4	23.4	23.3	23.2
Volumetric flow rate	m^3/s	1.7	1.71	1.88	1.91	1.91
Power output	W	390	393	431	437	435
Power input	W	987	938	889	838	790
Total efficiency		0.395	0.419	0.485	0.521	0.551

Next , the experiments are performed with the set-up which is raised 360 millimeters above the ground . Furthermore , the width of the steel plate on which the electric motor is mounted is decreased to 285 millimeters . Because the plate covers relatively less space in front of the fan , there is relatively more air air entering into the fan . Moreover , the length of the duct is increased by 450 millimeters at the inlet of the fan as shown in Figure 5.1 . All of these modifications on the test set-up results in an improvement in the air inlet conditions . The results obtained from these experiments are tabulated in Table 5.2 .

When compared with the case having poor inlet conditions , there is nearly 4 percent increase in the total pressure rise and 5 percent in the volumetric flow rate determined from the tests with improved inlet conditions . Also there is

nearly 11 percent increase in the power output as compared with the values determined from the tests with poor inlet conditions .

The performance curves of the axial fan are drawn according to the results obtained from the experiments with poor and improved inlet conditions . These curves are illustrated in Figures 5.2 to 5.9 . The curves corresponding to the poor inlet conditions are illustrated in Figures 5.2 to 5.5 . Figures 5.6 to 5.9 illustrate the performance curves of the axial fan with the improved air inlet conditions .

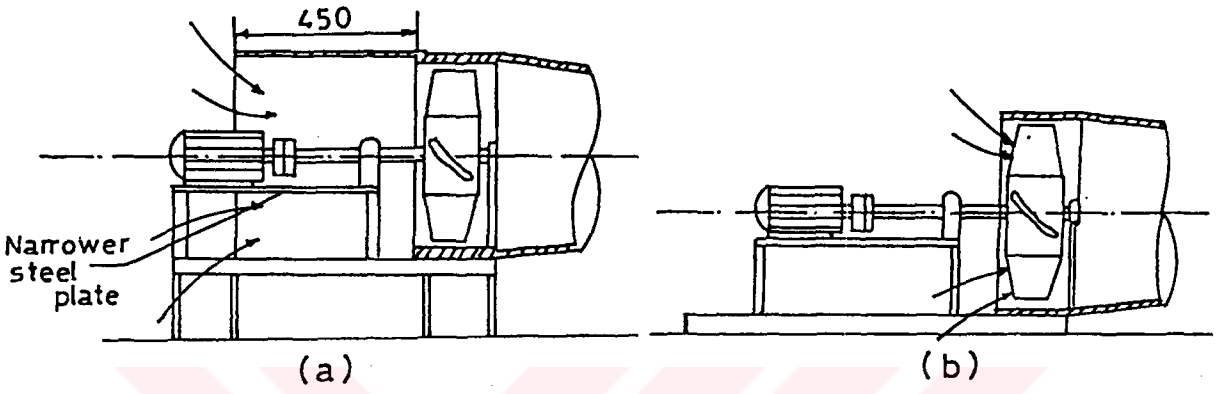

Figure 5.1 Modifications on the set-up (a) modified set-up (b) previous set-up

Table 5.2 The results of the performance tests with improved inlet conditions

MEASUREMENT NO		1	2	3	4	5
Static pressure inc.	Pa	230.3	230.3	230.3	222	212.2
Dynamic pressure inc.	Pa	15.3	14.7	14.6	15.0	15.3
Total pressure inc.	Pa	245.6	245	244.9	237.0	227.5
Static head	mmWG	23.5	23.5	23.5	22.6	21.7
Dynamic head	mmWG	1.6	1.5	1.4	1.5	1.5
Total head	mmWG	25.1	25.0	24.9	24.1	23.2
Volumetric flow rate	m^3/s	1.82	1.87	1.94	1.99	2.00
Power output	W	446	458	475	470	455
Power input	W	987	939	888	839	827
Total efficiency		0.452	0.488	0.535	0.560	0.550

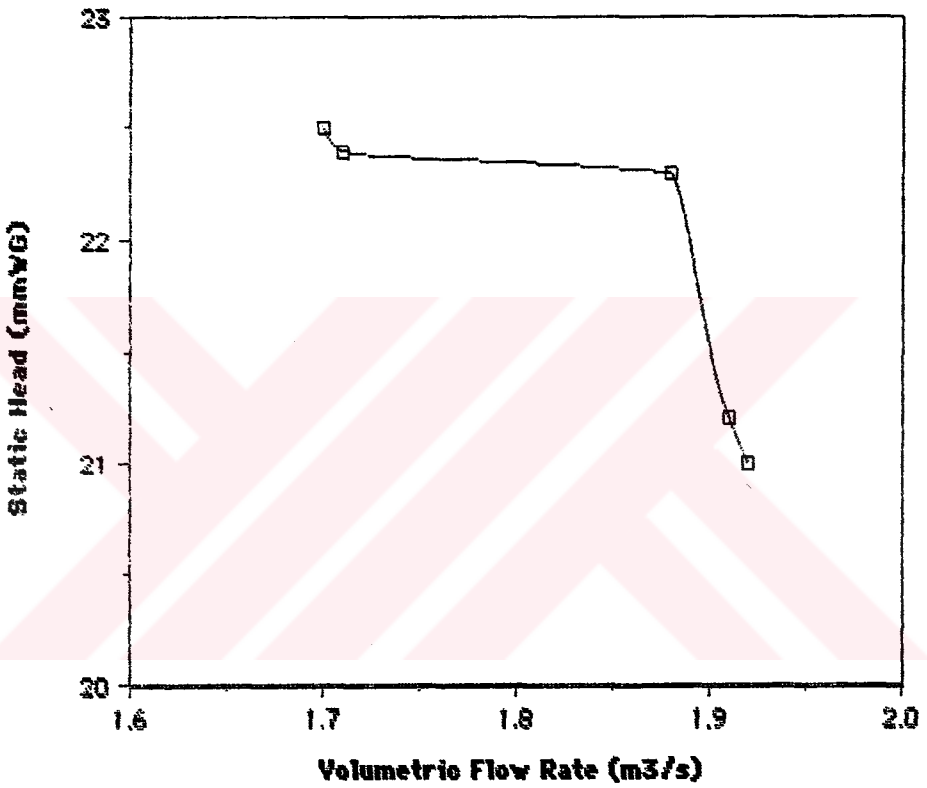

Figure 5.2 Static head versus volumetric flow rate graph
(Poor inlet conditions)

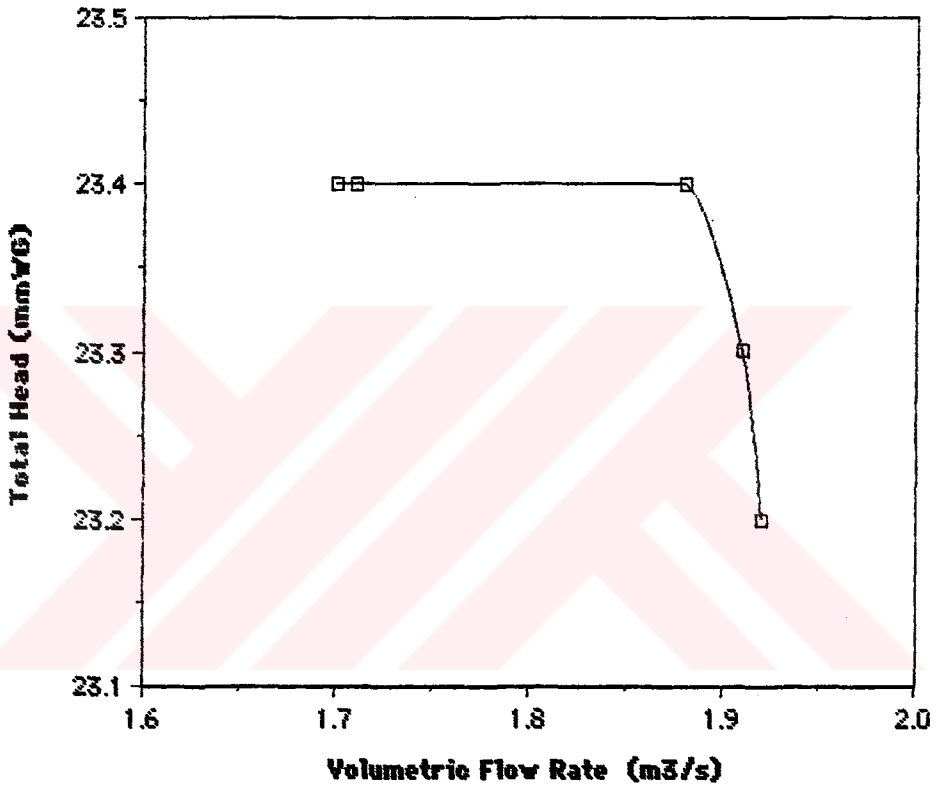

Figure 5.3 Total head versus volumetric flow rate graph
(Poor inlet conditions)

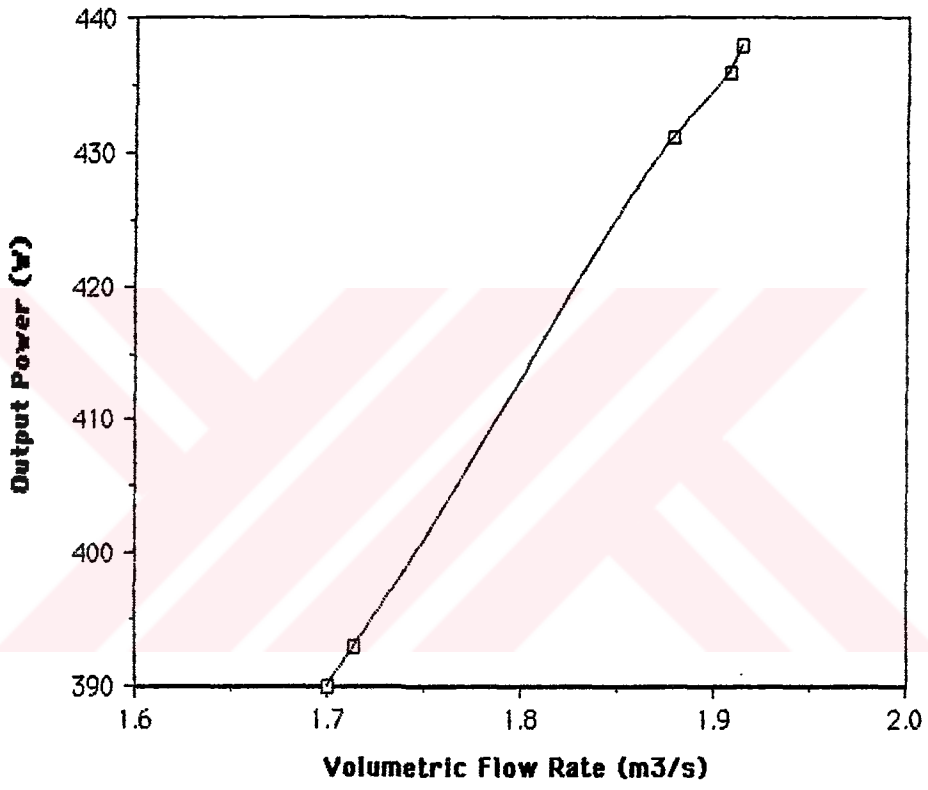

Figure 5.4 Power output versus volumetric flow rate graph
(Poor inlet conditions)

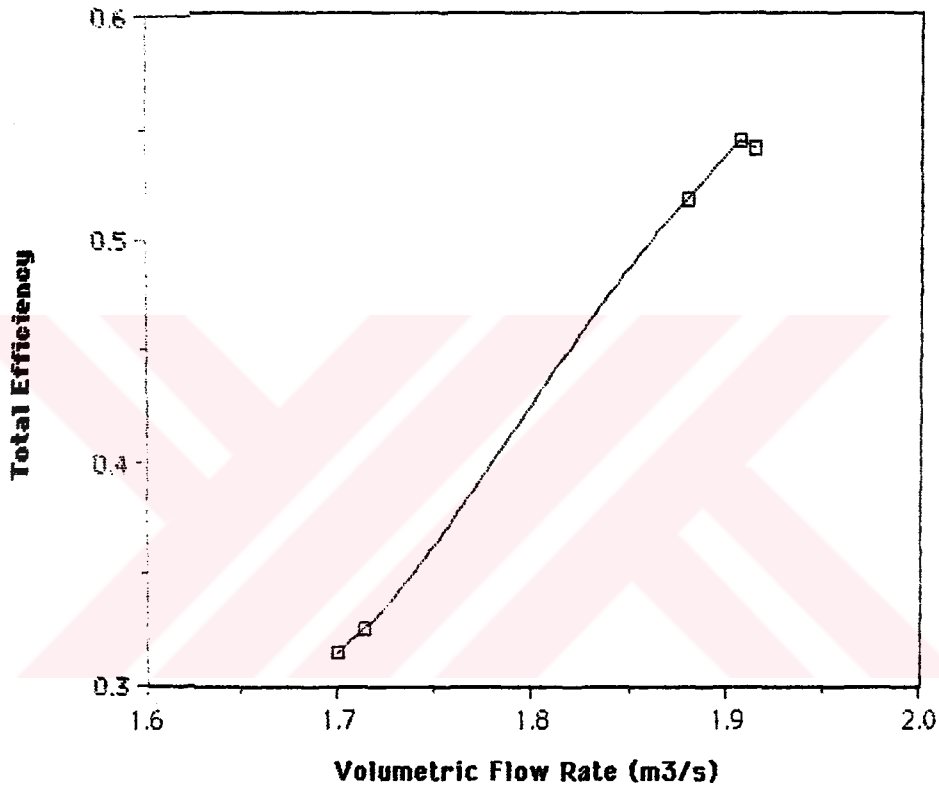

Figure 5.5 Total efficiency versus volumetric flow rate graph
(Poor inlet conditions)

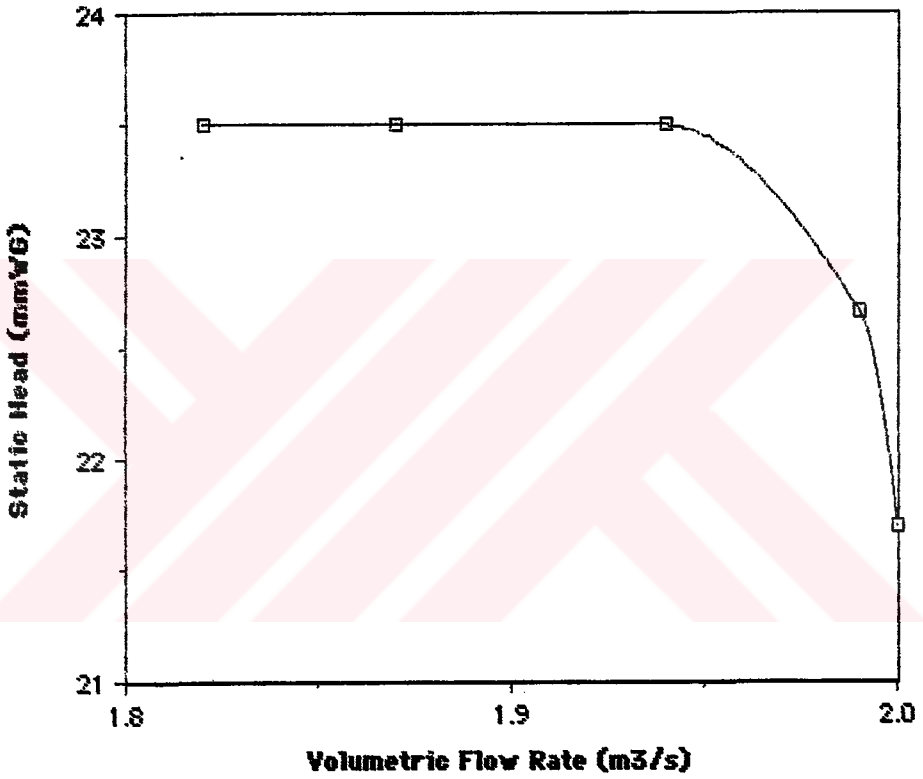

Figure 5.6 Static head versus volumetric flow rate graph
(Improved inlet conditions)

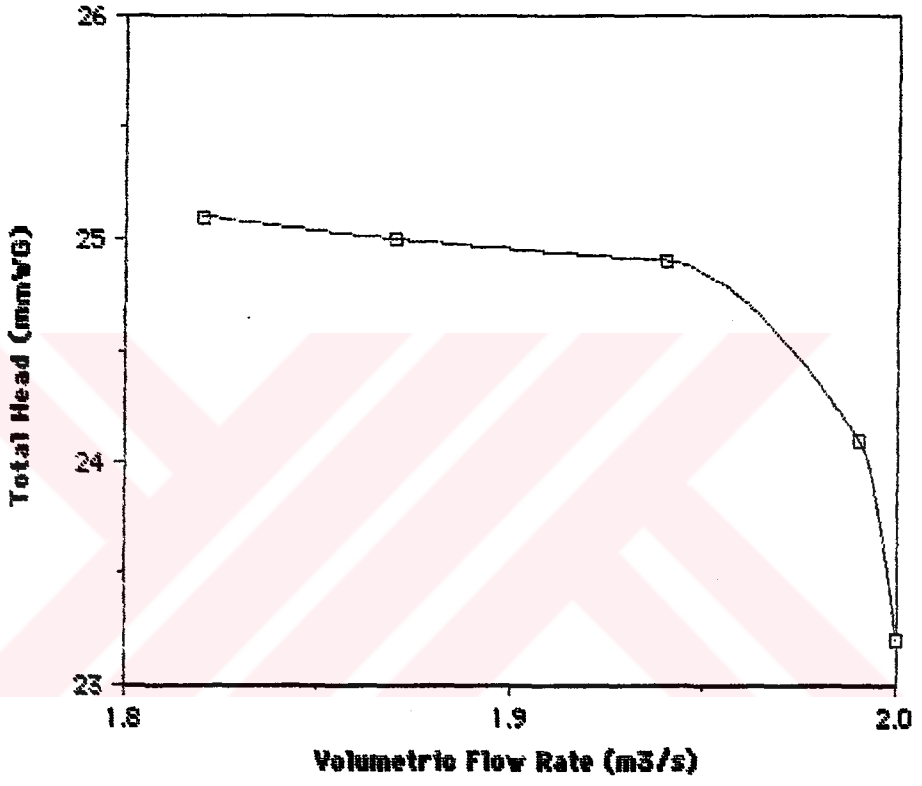

Figure 5.7 Total head versus volumetric flow rate graph
(Improved inlet conditions)

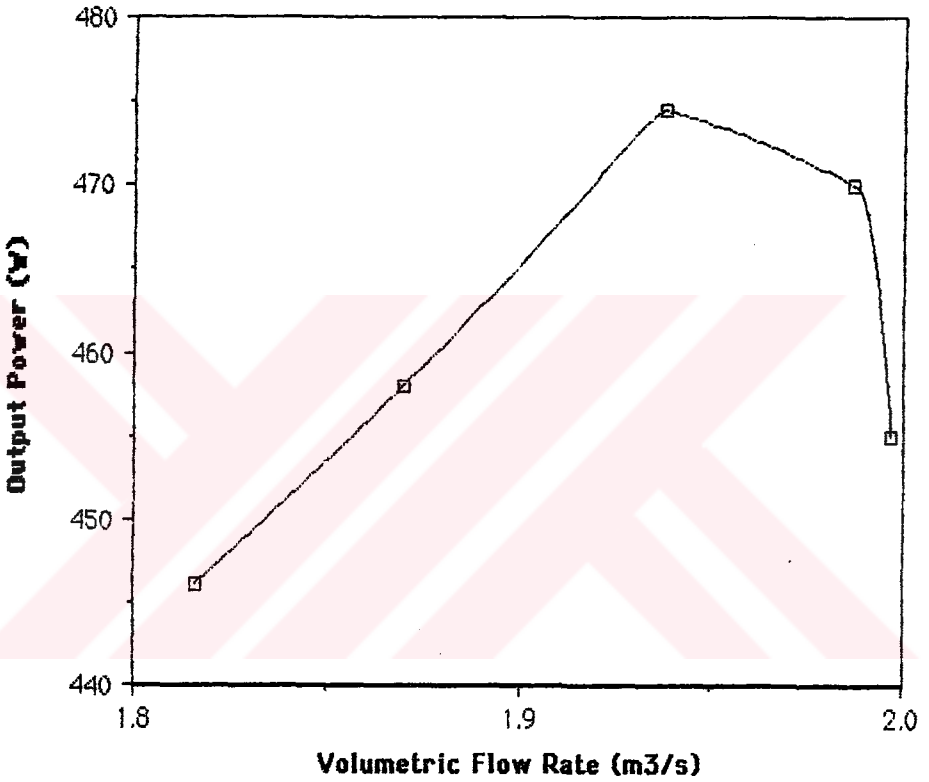

Figure 5.8 Power output versus volumetric flow rate graph
(Improved inlet conditions)

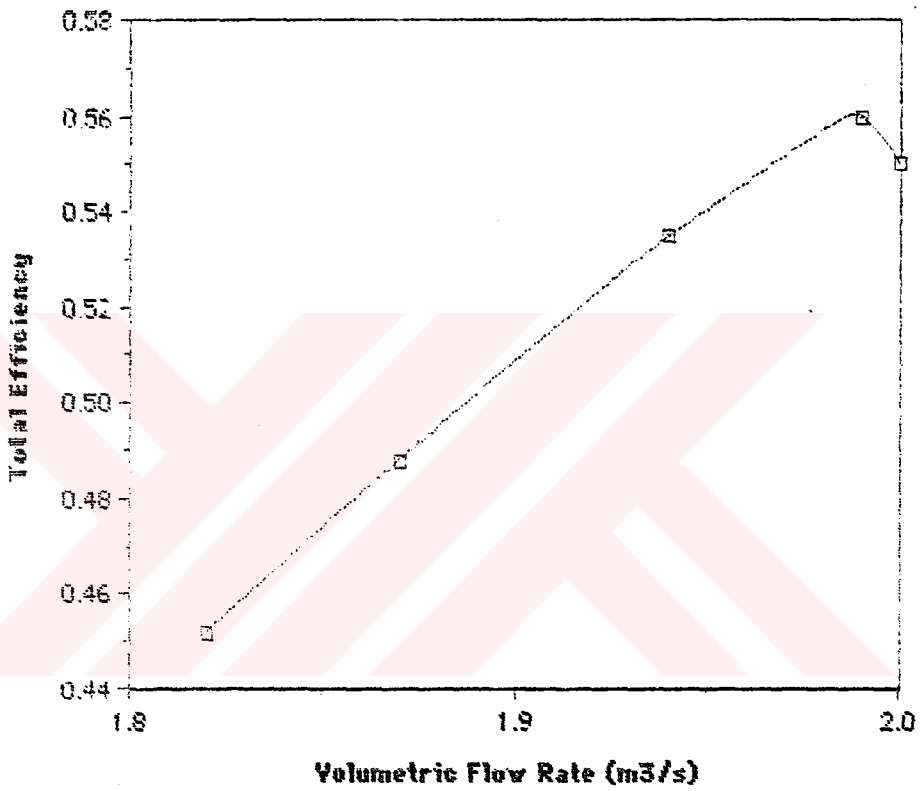

Figure 5.9 Total efficiency versus volumetric flow rate graph
(Improved inlet conditions)

CHAPTER VI

CONCLUSION

6.1 Discussion

As it is stated before , an axial fan is designed , manufactured and tested under standard performance evaluation techniques in this study . The axial fan design calculations are performed according to the procedure which is explained step by step in Chapter II . Due to the fact that in the design steps , more number of the divisions for the diameter ; that is more calculations for different diameters are recommended for the accuracy and the effectiveness , a computer code is needed to decrease the time for the design operations and to give accurate results . The computer code uses QBASIC Programming Language . The computer code not only performs the design calculations but also gives the drawings of the top and the side view of the axial fan . It also gives the blade orientations at different divisions and the cross-sectional view of a blade at the hub side . After the design calculations are performed , the manufacturing of the axial fan is started by using the design results obtained from the output of the computer code . Manufacturing operations consist of two phases , namely modelling and sand casting of the fan . Owing to its physical and strength characteristics , the fan is casted from Aluminum . As a final step , the performance of the manufactured axial fan is evaluated according to ASHRAE (American Society of Heating Refrigerating and Air Conditioning Engineers) Standard 51-75 . The performance tests are repeated several times in order to determine the performance curves of the fan correctly and accurately .

The computer code is run with the given input parameters namely , the total pressure increase , volumetric flow rate and the rotational speed . The dimensions required for manufacturing are taken from the computer output . After the performance evaluation of the fan , it is observed that there are some deviations from the design variables . These deviations are tabulated in Table 6.1.

Table 6.1 Deviations between the designed and tested variables

PERFORMANCE VARIABLE		Design	Test	Deviation
Total pressure inc.	Pa	250	240	4%
Volumetric flow rate	m^3/s	2.5	1.92	23%
Output power	W	746	461	38%
Total efficiency		0.87	0.53	39%

The reasons for the deviations between the designed and experimental values of performance variables are as follows :

i) The errors occured in the manufacturing steps :

It should be kept in mind that the modelling and casting of the fan requires special knowledge and capability . Since the model of the fan is hand-made , a small difference between the actual model and desired dimensions creates some error . As an example , the stagger angle , $\beta_{m'}$ is calculated as nearly 25 degrees at the tip and nearly 67 degrees at the hub side of the blade . These calculations are performed by the computer . However , on the model of the fan the angle , $\beta_{m'}$ is 27 degrees at the tip and 62 degrees at the hub side . Different runs of the computer code showed that because of a deviation in the angle , $\beta_{m'}$, there are some deviations in the performance variables of the manufactured fan . It is observed that slightly different $\beta_{m'}$ values are calculated by using the computer code with different input parameters . Another source of error can be the rough surface quality of the casted axial fan due to the sand casting process .

ii) The errors occured in the performance evaluation :

There may be some errors occured during the penetration of the Pitot tube into the duct . Since the location of the Pitot tube affects the pressure and the volumetric flow rate measurements , any deviation between the actual and desired location of the Pitot tube may cause an error in the performance variables . Furthermore , parts of the construction of the experimental set-up can affect the performance evaluation . For instance , the chasis on which the electric motor , housings and axial fan are mounted may affect the air inlet conditions in an undesired manner . For the minimization of these losses in the inlet conditions , the modifications on the construction of the chasis are done .

The deviations between the designed and experimentally obtained parameters may be decreased if the errors appeared in the manufacturing and performance evaluation steps are minimized .

There are also some deviations between the performance curves of the manufactured axial fan and the typical axial fan performance curves . The total head of the manufactured fan firstly remains constant and then decreases rapidly as the volumetric flow rate increases . The total head versus volumetric flow rate graph of a typical axial fan is a curve which increases gradually and decreases sharply as the volumetric flow rate increases . The total efficiency of the manufactured fan gradually increases and begins to decline sharply as the volumetric flow rate increases . The total efficiency versus volumetric flow rate curve of a typical axial fan has a steady rise and then a gradual decline . The power output versus volumetric flow rate curve of the manufactured fan has relatively sharp increases and decreases when compared to a typical one . These deviations are due to the errors occured in the manufacturing and performance evaluation of the axial fan . Also , the errors appeared when obtaining the operating points can affect the shape of the performance curves . As mentioned before , different autorities recommend that all of the excess curvature can be given to the blade outlet , being the blade inlet unchanged . The design procedure used in this study approximately halves the excess curvature and distributes nearly equal portions of

curvature to the blade inlet and to the blade outlet . Thus , this operation can be considered as an error source . The error analysis for the fan performance variables is in Appendix A . Also , in Appendix B , the calculation of the rotational speed to obtain the design parameters is illustrated .

6.2 Recommendations for Further Work

Obviously , this project will have a leading role for further researches in this field . The improvements in the design procedure , manufacturing and also performance evaluation steps in the further studies will increase the efficiency . As an eample , different experimental studies may be referred for the design calculations and non-traditional manufacturing processes can be used during the manufacturing of the axial fan . The casting molds of the blade and the axial fan can be manufactured with fine surface qualities and high tolerances by using one of the non-traditional machining processes , namely Electric Discharge Machining (EDM) . This process uses electric discharge as a heating energy . As a result of very high local temperatures like 12000 K , all electrically conductive materials can easily be machined since this temperature is higher than melting and evaporation temperatures of all materials . The previously shaped male electrodes are used to machine the workpiece which is generally a die or a mold . The occurence of very frequent electric sparks causes the material to melt and evaporate . Therefore , the workpiece is machined as the female shape of the electrode . Different electrodes are used for roughing , semi-finishing and finishing purposes . The electrode of the electric discharge machine can be shaped like an axial fan blade . Then , this electrode can be used to machine the mold of the blade . Making complex molds and cavities are costly and time consuming operations of the conventional techniques . EDM provides a reduction in time and cost by a considerable amount . Also , Wire Electric Discharge Machining (WEDM) which has nearly same operation principle with EDM can be used to manufacture dimensionally accurate axial fan blades . WEDM uses a moving wire made of electrically conductive material , generally brass instead of an electrode . There exists a relative motion between the wire and the work piece . The moving wire acts as a saw and cuts the workpiece in the desired shape . The three dimensional profile of the axial fan blade can be manufactured accurately with the aid of WEDM .

REFERENCES

[1] Pfleiderer & Petermann , Akim Makinalari , 2 (1978)
[2] Pfleiderer & Petermann , Akim Makinalari , 3 (1978)
[3] B . Eck , Fans , 54 (1973)
[4] R . Pollak , Chemical Engineering , Fluid Movers : Pumps , Compressors , Fans and Blowers ed . , 92 (1979)
[5] R . A . Wallis , Axial Flow Fans and Ducts (1983)
[6] B . Eck , Fans , 228 (1973)
[7] B . Eck , Fans , 242 (1973)
[8] B . Eck , Fans , 63 (1973)
[9] B . Eck , Fans , 254 (1973)
[10] Buhning , Concerning the Behaviour of Extreme High Speed Axial Machines , (1957)
[11] H . Marcinowski , Optimum Problems in Axial Flow Fans , 76 (1957)
[12] B . Eck , Fans , 225 (1973)
[13] B . Eck , Fans , 264 (1973)
[14] B . Eck , Fans , 263 (1973)
[15] Y . Shemoyama , Experiments with Rows of Aerofoils for Retarded Flow , 104 (1938)
[16] B . Eck , Fans , 287 (1973)
[17] B . Eck , Fans , 546 (1973)
[18] E . P . De Germo , J . T . Black , R . A . Kohser , Materials and Processes in Manufacturing , 251 (1984)

APPENDIX A

APPENDIX A

ERROR ANALYSIS

As mentioned before , during the performance tests various errors had occured . In this section , the percent errors in the

i) manometer deflection measurements
ii) static pressure calculations
iii) dynamic pressure calculations
iv) total pressure calculations
v) velocity calculations
vi) volumetric flow rate calculations
vii) fan power output calculations
viii) current measurements
ix) fan power input calculations
x) total efficiency calculations

are determined .

For Operating Point 1 , let ,

$$\Delta h_{stat} = x$$

The average value x is equal to

$$\bar{x} = \frac{x_1 + x_2 + x_3 + \ldots\ldots\ldots\ldots + x_n}{n}$$

The mean value x_m is equal to

$$x_m = \bar{x}$$

$$x_m = \frac{153 + 154 + 154 + 152 + 151 + 153 + 154 + 155 + 153 + 154}{10}$$

$$x_m = \bar{x} = 153.300 \text{ mm alcohol}$$

Then , the actual (calculated) value is calculated as,

APPENDIX A

$$[\sigma_a]^2=\frac{[x_1-x_m]^2-[x_2-x_m]^2+\ldots\ldots\ldots\ldots+[x_n-x_m]^2}{n}$$

$\sigma_a=1.1$

and ,

$$\sigma=\sigma_a\cdot\left[\frac{n}{n-1}\right]^{0.5}$$

$\sigma=1.1595$

The standard deviation is equal to ,

$$\sigma(\bar{x})=\frac{\sigma}{\sqrt{n-2}}$$

$\sigma(\bar{x})=0.4099$

Thus ,

$x=\bar{x}\mp\sigma(\bar{x})$

$x=153.300\mp0.4099$

The precision of the standard deviation is limitted by ,

$$S=\frac{\sigma(\bar{x})}{\sqrt{n-2}}$$

$S=0.145$

This means ,

$$\sigma(\bar{x})=0.4099\mp0.145\begin{cases}0.5549\\0.2649\end{cases}$$

The best estimate of the measured value can only be written by rounding off 0.4099 as

$x=153.3\mp0.4$ mm alcohol

Therefore ,

APPENDIX A

$\Delta h_{stat} = 153.3 \mp 0.4$ mm alcohol

or ,

$\Delta h_{stat} = 153.3 \mp 0.3\%$ mm alcohol

At this point the above calculations are done for the measurements of the manometer deflections which are performed to calculate the dynamic pressure values . After the similar calculations ,

$\Delta h_{dyn} = 10.3 \mp 2.9$ % mm alcohol

For the electrical current and voltage mesaurements ,

$I = 2.02 \mp 1.5\%$ A

$E = 380 \mp 1.3\%$ V

If Q is a quantity to be calculated by using parameters x_1 , x_2 , ..., that is if

$$Q[x_1, x_2, ...] = \overline{Q} + (\delta Q)$$

$$x_1 = x_1 \mp (\delta x_1)$$

$$x_2 = x_2 \mp (\delta x_2)$$

then the uncertainity in Q is calculated as follows ;

$$(\delta Q) = [(\frac{\partial Q}{\partial x_1} . \delta x_1) + (\frac{\partial Q}{\partial x_2} . \delta x_2) + ...]_{\overline{x}_1, \overline{x}_2, ...}$$

where δ is the uncertainity .

APPENDIX A

Using the above equation ,

$\Delta p_{stat} = 230.7 \mp 0.3\%$ Pa

$\Delta p_{dyn} = 15.6 \mp 3.2\%$ Pa

$\Delta p_{tot} = 246.2 \mp 0.5\%$ Pa

$V = 5.0 \mp 1.8\% \ \frac{m}{s}$

$Q = 1.81 \mp 2.2\% \ \frac{m^3}{s}$

$IP_o = 445.6 \mp 2.2\%$ W

$IP = 997.1 \mp 2.0\%$ W

$\eta_{tot} = 0.447 \mp 2.9\%$

This error analysis is done for the measured quantities only at the operating point 1 . The same calculations must be performed for the other operating points .

APPENDIX B

APPENDIX B

CALCULATION OF THE ROTATIONAL SPEED REQUIRED TO OBTAIN THE DESIGN PARAMETERS

As it is stated before , there are some deviations between the design and test performance variables . The deviation between the design volumetric flow rate and the test volumetric flow rate is nearly 23 percent . In order to find the rotational speed required to obtain the design volumetric rate and total head the following calculations are made :

$$H=C\cdot Q^2$$

where H is the total head , Q is the volumetric flow rate and C is a constant . In order to find the constant C , the design values of the total head and the volumetric flow rate are substituted into the above equation . Thus ,

$$H_D=25 \text{ mmWG}$$

$$Q_D=2.5 \ \frac{m^3}{s}$$

$$C=4.0$$

Thus ,

$$H=4\cdot Q^2$$

Firstly , $H= 4.Q^2$ curve is plotted on a millimetric paper . Then , H versus Q graph determined at the actual rotational speed is also plotted on the same paper . The intersection point of the two curves is designated as actual point , A . The fans at points A and D are similar but they are running at different rotational speeds . To find the rotational speed at design point , D ,

$$\frac{Q_A}{N_A}=\frac{Q_D}{N_D}$$

where subcript A designates the actual value and D designates the design value . From Figure A.1 , Q_A is found as 2.10 m^3/s . Then ,

APPENDIX B

$$\frac{2.10}{1400}=\frac{2.5}{N_D}$$

$N_D = 1667$ rpm

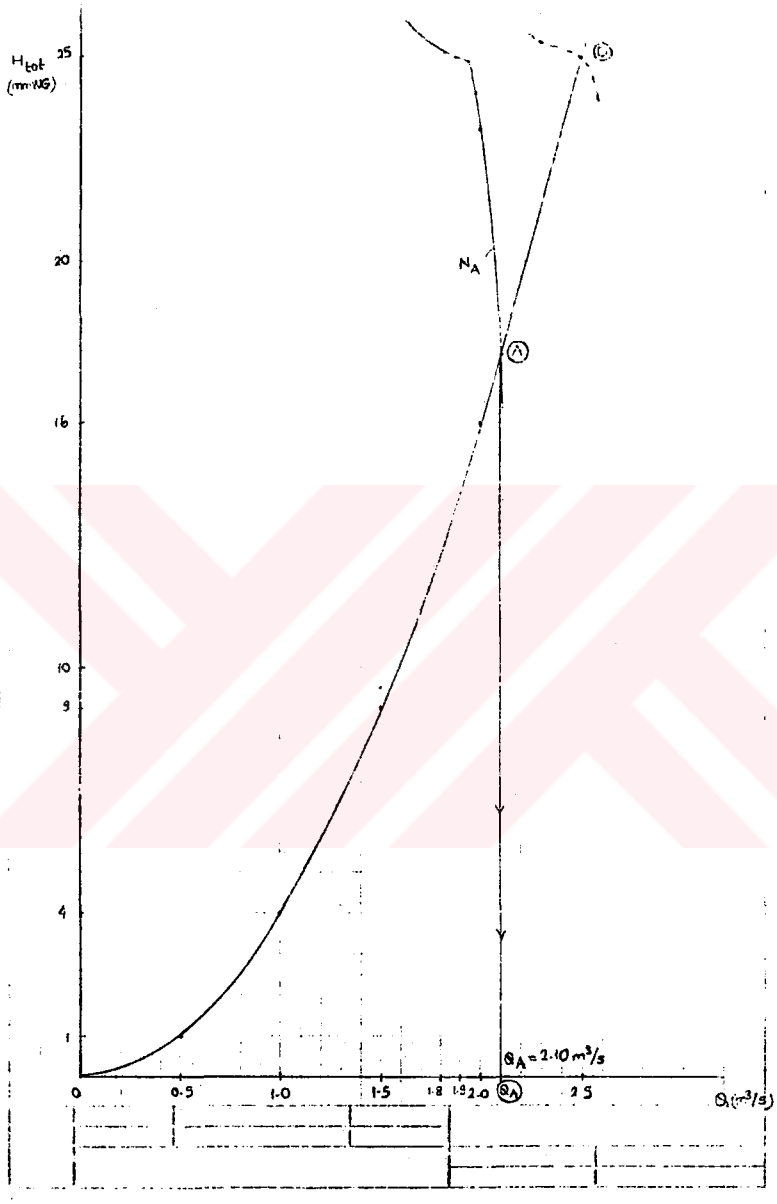

Figure B.1 $H=C.Q^2$ curve and H versus Q graph

Therefore , the manufactured axial fan has to be run at 1667 rpm to deliver the design volumetric flow rate (2.5 m^3/s) and the total head (25 mmWG) .